NASA CR 165241

NASA-CR-165241
19810018657

STRUCTURAL ANALYSIS OF CYLINDRICAL THRUST CHAMBERS FINAL REPORT VOLUME II

CONTRACT NAS3-21953

Prepared by

LOCKHEED MISSILES & SPACE COMPANY, INC.
HUNTSVILLE RESEARCH & ENGINEERING CENTER
HUNTSVILLE, ALABAMA

Prepared for

NATIONAL AERONAUTICS & SPACE ADMINISTRATION
LEWIS RESEARCH CENTER
CLEVELAND, OHIO

1. Report No.	2. Government Accession No.	3. Recipient's Catalog No.
NASA CR 165241		

4. Title and Subtitle	5. Report Date
STRUCTURAL ANALYSIS OF CYLINDRICAL THRUST CHAMBERS – Final Report – Volume II	March 1981
	6. Performing Organization Code
7. Author(s)	8. Performing Organization Report No.
W. H. Armstrong	LMSC-HREC TR D698400
	10. Work Unit No.
9. Performing Organization Name and Address	11. Contract or Grant No.
Lockheed Missiles & Space Company, Inc. P.O. Box 1103 Huntsville, Alabama 35807	NAS3-21953
	13. Type of Report and Period Covered
12. Sponsoring Agency Name and Address	Final Report
National Aeronautics & Space Administration Lewis Research Center Cleveland, Ohio 44135	14. Sponsoring Agency Code

15. Supplementary Notes

H. J. Kasper, NASA Technical Monitor

16. Abstract

Analytical results are presented which predict cumulative plastic deformation characteristic of damage observed in coolant channel walls of regeneratively cooled rocket thrust chambers. The damage consists of bulging and plastic flow which lead to thinout and rupture of the channel wall under the combined effects of high pressures, high temperatures and temperature gradients experienced during cyclic firings of actual test chambers. Analytical predictions correlate with test results.

17. Key Words (Suggested by Author(s))	18. Distribution Statement
Thrust Chamber Nonlinear Analysis Finite Element Analysis	Unclassified – Unlimited

19. Security Classif. (of this report)	20. Security Classif. (of this page)	21. No. of Pages	22. Price*
Unclassified	Unclassified	56	

* For sale by the National Technical Information Service, Springfield, Virginia 22161

NASA-C-168 (Rev. 10-75)

N81-27195 #

FOREWORD

This final report was prepared by Lockheed Missiles & Space Company, Inc., Huntsville, Alabama, for Lewis Research Center (LeRC), National Aeronautics and Space Administration, Cleveland, Ohio. The analytical evaluation of finite deformations of rocket engine test chambers subjected to constant amplitude thermomechanical loading cycles was conducted in accordance with requirements of Contract NAS3-21953 "Structural Analysis of Cylindrical Thrust Chambers." The study was under the cognizance of H. J. Kasper of NASA-LeRC and is a continuation of a previous effort reported in Ref. 1.

The analyses and documentation of results were conducted by W. H. Armstrong.

CONTENTS

1. SUMMARY

The objective of this study was to analytically determine the cumulative plastic deformation characteristic of damage observed in coolant channel walls of regeneratively cooled rocket thrust chambers. The damage of the channel wall consists of bulging and plastic flow which leads to thinout and rupture of the channel wall under the high pressures and high temperatures and temperature gradients experienced during successive cyclic firings of the thrust chamber. The study involves the structural analyses of LeRC test chambers of the same geometric configuration but constructed from different copper alloys.

The applied thermomechanical loading cycle was assumed constant in amplitude and period. Axisymmetric structural temperature and pressure load histories were provided by LeRC.

Structural response to the provided loading cycle was determined with the use of the BOPACE finite element computer program. Generalized plane-strain elements were used to model and analyze quasi three-dimensional behavior of the throat region of the thrust chambers. A computer program was developed (Ref. 2) for extrapolating BOPACE results. This program automates the manual extrapolation method employed in the study described in Ref. 1. The extrapolation method was developed to estimate finite deformation and low cycle fatigue damage in hot structures without a complete BOPACE cycle-by-cycle analysis over the life of the structure. The method provides a predictor-corrector technique wherein BOPACE computed deformations are used to predict configuration changes over a user specified number of loading cycles. The predicted configuration is analyzed in BOPACE and the computed deformations in the deformed model are read by the extrapolation program to establish another selected state of the deformed model. The procedure may be repeated as required.

Results are presented which show calculated permanent distortions of the chamber walls; nodal displacement plots of the hot gas and coolant surfaces and channel wall thicknesses as functions of number of loading cycles are included.

2. INTRODUCTION

Life predictions of regeneratively cooled rocket thrust chambers are normally derived from classical material fatigue principles. The failures observed in some experimental thrust chambers do not appear to be due entirely to material fatigue. The chamber coolant walls in the failed areas exhibited progressive bulging and thinning during cyclic firings until the hoop stress in the wall exceeded the material rupture stress and failure occurred. This is not to imply that the primary cause of failure is simply a case of applied stress exceeding the material strength in the deformed chamber. The large strains evidenced by plastic flow in the failed areas obviously result in material damage as well as thinout of the coolant wall. The failure mechanism possibly consists of the development of a low cycle fatigue crack which grows rapidly to a critical flaw size in the thinned wall. Consequently, analytically tracing the chamber wall thinout and changes in coolant passage geometry are important factors when attempting to predict thrust chamber life.

The study contained herein provides results of analyses of thrust chambers with OFHC copper, half-hard Amzirc and NARloy-Z liners. The analytical models were subjected to the same thermomechanical load environment to study cumulative geometric changes in the structures after several hundred operational cycles. Additionally studies were performed to determine material strain hardening and softening effects.

The OFHC copper chamber model was selected to determine a critical hot gas wall geometry for rupture in hoop tension and to compare the stress-critical configuration with a strain-critical configuration based on the instability point in a uniaxial tension test.

Finite displacements of the OFHC copper chamber were also used to evaluate changes in the structural temperatures in deformed configurations. This task was included to investigate the need to periodically update temperatures in the loading cycle for better convergence to total cumulative deformation.

3. PLUG NOZZLE THRUST CHAMBER

The structure analyzed during this study is the cylinder of a plug type thrust chamber shown in Fig. 1. The plug nozzle assembly consisting of the contoured centerbody and flanged cylinder is shown along with cross-sectional details of the cylinder. The contoured centerbody provides a variable cross section area along the length of the cylinder similar to that which exists in a conventional contoured thrust chamber.

The basic component of the cylinder is the inner wall which contains 72 axial flow coolant channels of constant cross section. Three basic cylinders were modeled and analyzed. One cylinder inner wall was constructed from half-hard Amzirc, one from NARloy-Z and one from OFHC copper. The closeout wall of the basic configurations was electroformed copper (EFCU). A second OFHC copper configuration with an electro-deposited nickel (EDNi) closeout wall was also modeled and analyzed.

3.1 THRUST CHAMBER MATERIAL PROPERTIES

The properties used to characterize the cylinder wall materials were provided by LeRC. The data, taken from Ref. 3, define typical temperature dependent thermal expansion, modulus of elasticity and static stress-strain properties of half-hard Amzirc, NARloy-Z, annealed OFHC and EFCU. The material properties are presented in Figs. 2 through 16.

3.2 THERMOMECHANICAL LOADING CYCLES

The loading applied to the cylinder model consisted of constant amplitude thermomechanical cycles. A baseline cyclic load applied in 24 increments of temperature and pressure was supplied by LeRC.

A second thermal cycle based on data presented in Ref. 4 was also applied to the OFHC/EFCU and OFHC/EDNi models. The second cycle identified as SN34 in Ref. 4 resulted in a general increase in inner wall temperatures and a decrease in the closeout wall during the heating phase of the cycle. The radial temperature gradient is greater in the second cycle. Pressure histories were the same for both cycles.

The loading was assumed axisymmetric and structural symmetry was exploited in order to treat the smallest representative segment of the chamber. The operating pressures defined in Fig. 17 were applied to the hot gas surface and coolant channel and were assumed to vary linearly with time during transition periods between cooling and heating phases. The duration of each transition period as well as the durations of cooling and heating phases were specified and are defined in Fig. 17.

Baseline temperature histories at selected throat plane nodes of the analytical model are shown in Fig. 18. The origin of the time scale, i.e., time = 0 on this plot is the beginning of the hot phase shown on the diagram accompanying Fig. 17. SN 34 temperature histories are shown in Fig. 19 for comparison of the two cycles.

4. STRUCTURAL ANALYSIS

A quasi three-dimensional structural analysis of the thrust chambers was performed with the BOPACE finite element computer program. Generalized plane-strain isoparametric elements were used to model the smallest repeating segment of the cylinder wall, and time-varying nodal temperatures, elemental pressure loading and axial thermal strains were applied to compute chamber wall deformation histories under repetitive firing cycles. In addition, nonlinear variations in the temperature dependent material properties and mechanically and thermally induced plasticity were accounted for in the computations.

A system of three computer programs (Ref. 2) was also developed for use with BOPACE. An extrapolation program was developed to predict finite element model nodal displacements over a range of cycles by using BOPACE computed nodal displacements. A plot package was developed to display predicted configurations, and a BOPACE restart tape reader routine was included for retrieving the computed nodal displacements from BOPACE restart tapes for extrapolation or plotting.

The extrapolation method was developed to estimate finite deformation and low cycle fatigue damage in hot structures without a complete BOPACE cycle-by-cycle analysis over the life of the structure. The method provides a predictor-corrector technique wherein BOPACE computed deformations are used to predict configuration changes over a specified number of loading cycles. The predicted (deformed) configuration is then analyzed in BOPACE and the computed deformations in the deformed model are read by the extrapolation program to establish another selected state of the deformed model. The procedure may be repeated as required.

The extrapolation procedure utilized a linear least squares approximation to establish the computed displacement rate of each node in the finite element model. The program provides the option of extrapolating up to and including three components of the computed nodal displacement vector. The input and output of the extrapolation program are compatible with BOPACE Version 6.0. Card input/output is used as the transfer medium between BOPACE, the extrapolation program and the plotting program. This provides the user with complete flexibility in the choices of configurations to plot, extrapolate and feed back to BOPACE for additional computation. Examples of the extrapolation procedure are presented in Ref. 2.

An initial chilldown from an assumed fabrication temperature of 294 K (530 R) to a uniform 28 K (50 R) with appropriate coolant surface pressure was applied to simulate initial starting conditions in the test thrust chambers. The entire chamber model remained elastic during the initial chilldown.

Ten identical firing cycles were then imposed on each of the chamber models which were geometrically the same prior to initial chilldown. Three-dimensional behavior of the chambers was approximated by specifying a time varying axial strain equal to the average thermal strain of the relatively massive closeout wall. The BOPACE solution involved load incrementation, periodic updating of the stiffness matrix and residual load iteration to ensure equilibrium.

The cumulative deformations at the end of a firing cycle were used as the referent configuration for the succeeding cycle. The entire structure was at 28 K (50 R) with a coolant channel pressure of 5.1 MPa (740 psia) at the end of each cycle. The computed volume of the 10th cycle configurations was used to check extrapolated configurations to assure that total mass was conserved during the analysis.

A schematic of the chamber model is shown in Fig. 20. Node and element numbers are identified. The inner wall region is comprised mainly of quadratic

elements. Higher order elements were used on the hot-gas and coolant boundaries in an attempt to more accurately determine nodal displacements on these two surfaces. The closeout wall which exhibits no significant plastic deformation was modeled with linear elements. A computer plot of the undeformed model is presented in Fig. 21.

4.1 HALF-HARD AMZIRC AND NARLOY-Z CHAMBER RESULTS

The Amzirc and NARloy-Z chamber models with EFCU closeout walls were subjected to the baseline thermomechanical load cycle. The first 10 firing cycles were consecutively applied after initial chilldown in the BOPACE code.

It was observed that no apparent thinning or bulging of the NARloy-Z channel wall was predicted over the first 10 cycles, and the analysis of the NARloy-Z configuration was discontinued. Apparently the loading cycle was not severe enough to cause significant finite deformation in the NARloy-Z chamber although an effective strain range of 1.8% per cycle was predicted in the inner wall region.

Nodal displacements of the Amzirc chamber were used to define displacement rates of all nodes within the BOPACE model at the end of the 10th cycle. These rates were extrapolated to 50 cycles and the deformed configuration nodal positions were supplied to the BOPACE code to redefine the model and perform an additional set of five thermomechanical load cycle analyses to establish nodal deformation rates of the Amzirc 50-cycle configuration. This procedure was repeated until the Amzirc model exhibited no further apparent finite deformation in the inner wall.

The initial thickness of the channel wall was 0.0889 cm (0.035 in.) at room temperature and 0.08854 cm (0.03486 in.) at the end of the initial chilldown. The Amzirc analysis was extended in 50 cycle increments to 150 cycles. The predicted thickness of the inner wall is shown in Fig. 22. The analytical model of the Amzirc chamber exhibited no apparent thinout beyond 100 cycles. Profiles of the deformed hot-gas and coolant wall of the 100-cycle configuration of the Amzirc chamber are shown in Fig. 23.

It was assumed that the Amzirc material was stable throughout the cyclic range, i.e., no isotropic hardening or softening was characterized and no change in kinematic hardening was assumed. Also the loading cycle was constant throughout the range of investigation.

Although some plastic flow and bulging of the inner wall of the model are apparent, they were small relative to predicted behavior of the OFHC copper chamber. This prediction is consistent with damage observed in actual test chambers and suggests that the environment was not severe enough to result in deformation and rupture of the Amzirc. The environment does cause low-cycle fatigue leading to crack formation predictable from low-cycle fatigue life curves developed for the predicted strain and temperature ranges in the inner wall. The computed effective strain range is 1.6% per cycle, and the predicted cyclic life is 2200 cycles.

4.2 OFHC/EFCU AND OFHC/EDNi CHAMBER RESULTS

Two different load cycles were applied to the OFHC/EFCU chamber models. The procedure was the same as used to analyze the Amzirc configuration except the extrapolation was performed in 25-cycle increments.

Results of the analyses using the baseline thermal cycle are summarized in Figs. 24 through 28. Figure 24 shows inner wall thickness over a 200 cycle range and indicates no apparent thinning of the inner wall between 150 and 200 cycles. The initial and final wall thickness at the channel centerline were 0.0889 cm (0.035 in.) and 0.0701 cm (0.0276 in.), respectively.

Figures 25 and 26 show the profiles of the hot gas and coolant walls of the 100-cycle and 200-cycle configurations of the analytical model. The predicted plastic flow and bulging are consistent with qualitative results from OFHC test chambers. Computer plots of the 100 and 200 cycle OFHC/EFCU configurations are presented in Figs. 27 and 28.

The second load cycle consisting of the same pressures as used in the baseline but using the temperature cycle designated as SN 34 (Ref. 4) was applied to the OFHC/EFCU model.

Effects of the SN 34 cycle were determined by analyzing the first 10 consecutive cycles. The nodal displacement rates were extrapolated in 50 cycle increments to 200 cycles. The wall thickness history of the OFHC/EFCU chamber model is shown in Fig. 29. The final thickness of the OFHC/EFCU inner wall was predicted to be 0.0740 cm (0.02915 in.). Although this is a greater thickness than predicted for the baseline cycle, the SN 34 cycle is potentially more damaging because the wall thinout is accelerating and could result in an unstable structure subject to rupture.

An OFHC inner wall model with an EDNi closeout was analyzed for 10 consecutive SN 34 load cycles. It was necessary to determine the structural temperatures for this model because of the heat conduction characteristics of the new closeout wall. The heat conduction analysis was performed with the NASTRAN code and the nodal temperature histories were supplied to the BOPACE model. Boundary conditions and material properties used in the NASTRAN heat conduction analysis are shown in Fig. 30. Isotherms for the heating and cooling phases of the OFHC/EDNi SN 34 cycle are shown in Figs. 31 and 32. Computed temperature histories of the OFHC/EDNi chamber are presented in Fig. 33.

The inner wall thickness of the OFHC/EDNi model is shown in Fig. 34. The computed thickness after 10 cycles is 0.0868 cm (0.0342 in.) and the thinout rate is -0.0000254 cm/cycle (-0.00001 in./cycle).

Although the OFHC/EDNi model exhibited small geometric changes, the model does predict significant plastic strain in the inner wall. The computed effective strain range was 2.7% per cycle. Thus significant low-cycle fatigue damage would occur early in the life of this chamber. The predicted number of cycles to crack initiation in the OFHC chamber wall is 70 cycles (Ref. 3).

A more rigorous analysis of the OFHC/EDNi structural temperatures could result in a revised response to the SN 34 environment. Also the EDNi material properties used in the thermal analysis may warrant further investigation. The EDNi thermal properties were obtained from Ref. 5.

4.3 DETERMINATION OF OFHC/EFCU CRITICAL GEOMETRY AND COMPARISON WITH TENSILE INSTABILITY

The OFHC/EFCU model was used to determine a critical time within a cycle and the critical geometry of the inner wall which could result in tensile rupture of the channel wall. The procedure was to extrapolate the OFHC/EFCU model to various configurations and apply the baseline thermomechanical cycle to determine maximum hoop tensile stresses and times within the cycle of occurrence of the maximum stress condition. The nodal deformation rates at the end of 75 cycles were linearly extrapolated over a range of 175 cycles to obtain the severely thinned and bulged models used in this effort. For purposes of identification the deformed models were identified as configurations 1, 2 and 3 and possessed channel wall thicknesses of 0.0645 cm (0.0254 in.), 0.0549 cm (0.0216 in.) and 0.0455 cm (0.0179 in.), respectively. The computer models of configurations 1, 2 and 3 are shown in Fig. 35. The initial configuration, identified as 0, had a wall thickness of 0.0889 cm (0.035 in.).

BOPACE analyses of these configurations indicate that a maximum tensile hoop stress is induced in the channel wall approximately 0.26 sec after the start of shutdown (time = 1.81 sec) in the baseline cycle. Node 65, located on the centerline of the channel on the coolant side, is the critical location in the chamber wall and the conditions at this time at node 65 are a temperature of 139 K (250 R) and a typical uniaxial tensile strength of 303 MPa (44 ksi). The computed hoop stress histories of node 65 for each configuration are shown in Fig. 36. The computed hoop stress at node 65 at time = 1.81 sec is plotted against the channel wall thickness as presented in Fig. 37 which shows that rupture of the channel wall should occur in a thickness range of 0.0483 to 0.0559 cm (0.019 to 0.022 in.). The scatter band is probably larger because the BOPACE analysis does not account for variations in quantities such as tensile strength, strain or age hardening, temperatures, etc., but is considered a good estimate of conditions for incipient failure due to tensile rupture of the channel wall.

A hypothesis has been proposed that incipient rupture of the channel wall might be based on the strain at the point of instability in a uniaxial tension test.

The instability point in a simple tension test is defined as the point at which maximum load occurs, uniform straining ends and necking begins. The simple tension test therefore reaches its limit not at fracture, but at the maximum load condition. This failure criterion is based on several assumptions, the first of which is that the strain hardening exponent, n, in the equation of the inelastic portion of a uniaxial stress strain curve is a function of the tensile ultimate (F_{tu}) and yield strengths (F_{ty}) at a given uniform temperature. An approximation for n derived at LeRC is

$$n = 0.2\left(\frac{F_{tu} - F_{ty}}{F_{ty}}\right)^{0.6}$$

It has been observed that finite cumulative deformation in the OFHC chambers is very nearly a plane-strain effect. Thus the cumulative radial component of engineering strain defined by the ratio

$$\epsilon = (t_o - t_f)/t_o$$

where

t_o = original wall thickness
t_f = failure or instability thickness

is at least two orders of magnitude greater than the out-of-plane (axial) strain component. The incompressibility condition requires that the cumulative strains in the radial and circumferential directions at the channel centerline be equal. This condition leads to the equation

$$t_f = t_o\,(2 - e^{\bar{\epsilon}}) = t_o\,(2 - e^{n})$$

where

$\bar{\epsilon}$ = true strain.

n = $\bar{\epsilon}$ for uniaxial test specimen

Results presented at the beginning of this section show that the maximum tensile stress occurs in the channel wall 0.26 sec after the start of

shutdown when the channel wall temperature is 139 K (250 R). The corresponding tensile strengths of OFHC copper as reported in Ref. 2 are F_{tu} = 303 MPa (44 ksi) and F_{ty} = 62 MPA (9 ksi) with the result that $n = \bar{\epsilon} = 0.452$. The corresponding tensile instability thickness would then be

$$t_f = 0.0889\,(2 - e^{0.452})$$

$$= 0.0381 \text{ cm } (0.015 \text{ in.})$$

which compares to the previously reported unstable wall thickness defined by the scatter band of computed BOPACE data of 0.04826 cm to 0.05588 cm (0.019 in. to 0.022 in.).

It is concluded that the proposed method is possibly a lower bound to the tensile instability thickness and may achieve closer correlation with the BOPACE computed critical geometry with careful determination of typical temperature dependent tensile strengths used in computing the strain-hardening exponent. Also, the temperature history used in the BOPACE load cycle is of critical importance in computing the cumulative finite deformations of the channel wall.

4.4 CHAMBER STRUCTURAL ANALYSES WITH STRAIN SOFTENING AND STRAIN HARDENING EFFECTS

Models of hypothetical isotropic strain hardening and strain softening materials were prepared to evaluate the effect on plastic deformation in the inner wall. Although the models do not represent real materials, their assumed stress-strain properties are similar to the Amzirc alloy considered in this study. The material properties were assumed to vary linearly between the temperatures of 28 K (50 R) and 861 K (1550 R). The assumed hysteresis curves are shown in Figs. 38 and 39.

Four different BOPACE models were prepared to assess the effects of changes in isotropic hardening in the thrust chamber. These models all used EFCU as the closeout wall and were subjected to the baseline load cycle.

The four models were:

1. A stable "hard" model with temperature dependent properties defined by the major cycles.
2. A "softening" model with initial temperature dependent properties defined by the major cycles and final properties defined by the minor cycles. The softening effects were accelerated by assuming a linear variation (reduction) in strain energy density over a 5-cycle fixed-strain range of $\pm 1\%$.
3. A stable "soft" model with temperature dependent properties defined by the minor cycles.
4. A "hardening" model with initial temperature dependent properties defined by the minor cycles and final properties defined by the major cycles. The hardening effects were accelerated by assuming a linear variation (increase) in strain energy density over a 5-cycle fixed-strain range of $\pm 1\%$.

Results of the strain hardening study are presented in Fig. 40 which shows cumulative effective plastic strain range in element 16 of the BOPACE chamber model. Element 16 which is adjacent to the channel centerline on the coolant side is the element which exhibits the greatest cumulative plastic strain. Figure 40 shows that the strain softening material model exhibited the greatest sensitivity to the assumed isotropic strain effect; the effective strain range increased approximately 58% over the last four cycles. Although the effects were accelerated for this study, this behavior might occur in materials such as hardened Amzirc or NARloy-Z and could be analytically accounted for if the appropriate hysteretic temperature dependent material data were available to model these materials. It appears that the environment for the LeRC test chambers is not severe enough to result in significant plastic flow and distortion of the Amzirc and NARloy-Z chambers, but the low-cycle fatigue life based on cumulative strain damage of these two alloys may be much less than predicted from stable material models.

4.5 EFFECT OF OFHC/EFCU INNER WALL DEFORMATION ON STRUCTURAL TEMPERATURES

A study of the 100-cycle and 200-cycle configurations of the OFHC/EFCU chamber was performed to determine effects of finite dimensional changes on

inner wall temperature gradients. The baseline thermal environments for the initial configuration were applied to NASTRAN heat conduction models of the two deformed chambers and cyclic temperatures were computed.

A comparison of nodal temperatures at the end of the baseline heating phase for initial, 100-cycle and 200-cycle configurations is presented in Fig. 41. The maximum changes in nodal temperature with deformation occurred at node 65 where the computed temperature increased 11 C (20 F) and 30 C (55 F) over the baseline temperature for the 100-cycle and 200-cycle configurations, respectively.

The inner wall thickness at the channel centerline at the end of the heating phase was 0.0906 cm (0.03566 in.), 0.0766 cm (0.03018 in.) and 0.0717 cm (0.02823 in.) for the initial, 100-cycle and 200-cycle configurations, respectively. The computed radial temperature gradient at the channel centerline of the the respective configurations is 1085 K/cm (4964 F/in.), 1116 K/cm (5102 F/in.) and 1162 K/cm (5313 F/in.). This is only a 2.8% increase in the temperature gradient for a 15.4% decrease in thickness when going from the initial to the 100-cycle configuration. There was a 7.03% increase in temperature gradient for a 20.8% decrease in wall thickness at the end of heating at 200 cycles.

It appears that configuration changes predicted in the OFHC/EFCU model have a small effect on the overall model temperature field and do not warrant periodic updating of the temperatures in a cyclic life prediction analysis. The greatest effect is thought to result from a significant change in the average temperature gradient between the inner and closeout walls. The computed temperatures result in only 5.5 C (10 F) increase in the temperature gradient between points at the centers of the inner and closeout walls of the initial and 200-cycle models; this would have negligible effect on finite deformations and strains if spread uniformly over the 200-cycle range.

5. CONCLUDING REMARKS

A set of three computer codes was developed for use with the BOPACE finite element program for predicting cumulative deformation of structures subject to many thermomechanical load cycles. The program set consists of an extrapolation code, a plot package and a BOPACE restart tape reader routine.

The extrapolation method was developed to predict finite deformations and low-cycle fatigue damage in structures without performing a cycle-by-cycle finite element analysis over the life of the structure. The method provides a predictor-corrector technique wherein BOPACE computed deformations from several consecutive load cycles are used to predict configuration changes in the finite element model over a specified number of loading cycles. For example, the initial finite element model of the thrust chamber was subjected to 10 consecutive thermomechanical load cycles. The nodal displacements from BOPACE restart tapes for cycles 8, 9 and 10 were used in the extrapolation code to predict nodal displacements and coordinates out to 25 cycles. The 25-cycle configuration was analyzed in BOPACE to determine the rate-of-change in nodal displacements over 5 cycles. These corrected displacement rates were then used to predict a 50-cycle deformed model configuration. The procedure was repeated out to 200 cycles. The plot package permits the user to quickly examine the finite-element models after any selected number of cycles.

The extrapolation procedure uses a linear least squares approximation to establish the displacement rate of each node in the finite element model. The code provides the option of extrapolating up to, and including, three components of the nodal displacement vector. Card input/output is used as the medium of communication between BOPACE, the extrapolation code and the plot package. This provides the user with complete flexibility in choices

to plot, extrapolate and feed back to BOPACE for additional computation. The computer codes are fully documented (Ref. 2) with theory, user, programmer and example problem manuals.

Analytical predictions correlate with observed test results from the throat section of thrust chamber (Fig. 1) which were subjected to constant amplitude thermomechanical load cycles (Fig. 17). The OFHC/EFCU deformation history over 200 cycles was predicted using 25 BOPACE runs and 8 extrapolation runs; total BOPACE computer time was approximately 15 CPU hours on an IBM 370 system using 265 K bytes of core for each run. The extrapolations were run on a Univac 1100 system using 15 K words of core and approximately 4 minutes per run. The extrapolation procedure provided a significant reduction in computer time. A BOPACE cycle-by-cycle analysis of 200 load cycles applied to the OFHC/EFCU thrust chamber model would require approximately 70 CPU hours of computation on the IBM 370.

6. REFERENCES

1. Armstrong, W. H., "Structural Analysis of Cylindrical Thrust Chambers, Vol. 1," NASA CR-15922, Contract NAS3-21361, NASA-Lewis Research Center, Cleveland, Ohio, March 1979.
2. Pearson, M. L., "Structural Analysis of Cylindrical Thrust Chambers, Vol. III," NASA CR-165242, Contract NAS3-21953, NASA-Lewis Research Center, Cleveland, Ohio, December 1980.
3. Esposito, J. J., and Zabora, R. F., "Thrust Chamber Life Prediction — Mechanical and Physical Properties of High Performance Rocket Nozzle Materials," NASA CR-134806, Contract NAS3-17838, NASA-Lewis Research Center, Cleveland, Ohio, March 1975.
4. Quentmeyer, R. J., H. J. Kasper and J. M. Kazaroff, "Investigations of the Effect of Ceramic Coatings on Rocket Thrust Chamber Life," NASA TM-78892, NASA-Lewis Research Center, Cleveland, Ohio, July 1978.
5. Material Properties Manual, Rockwell International, Rocketdyne, Division, September 1977.

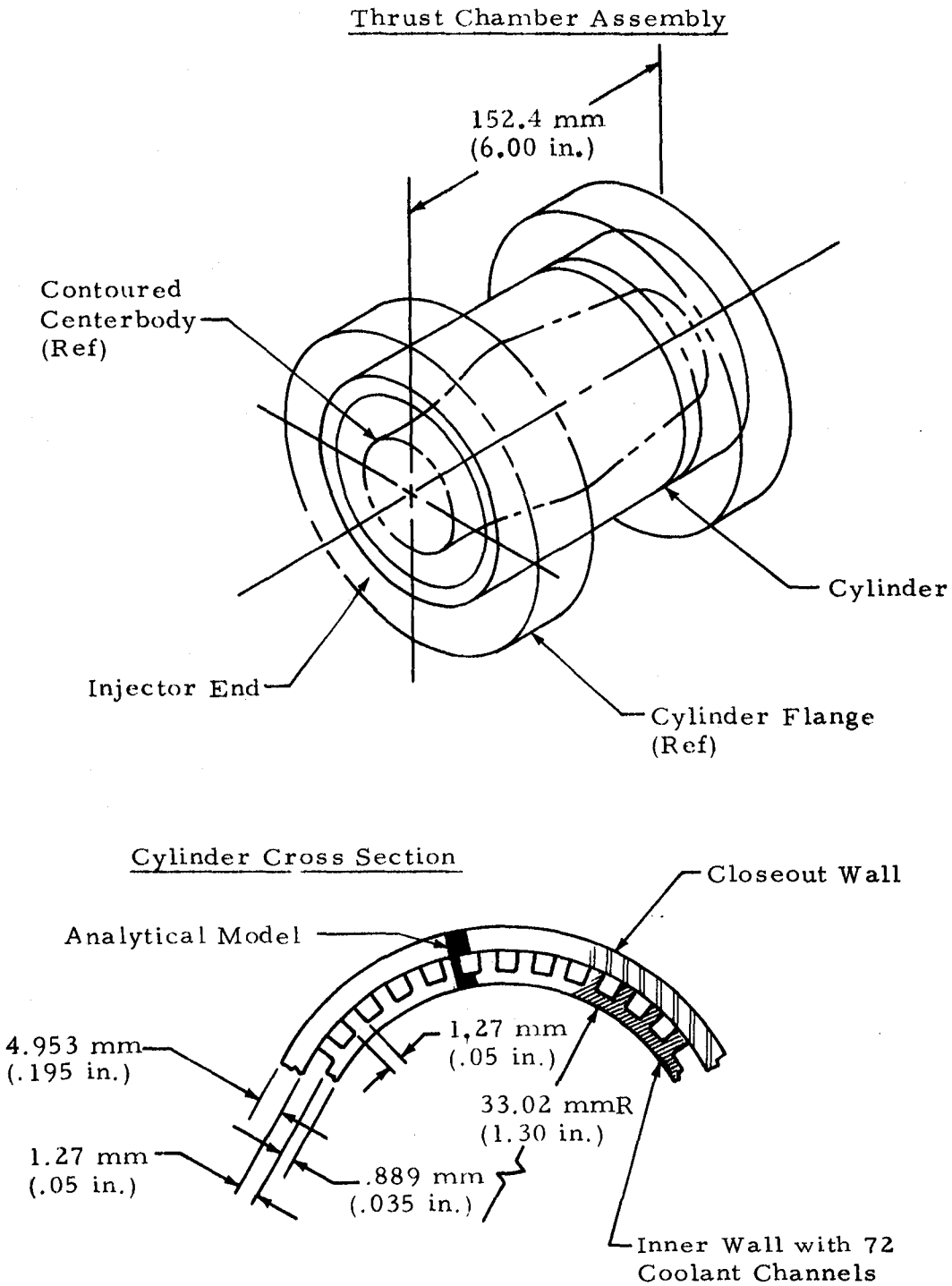

Fig. 1 - Plug Nozzle Thrust Chamber

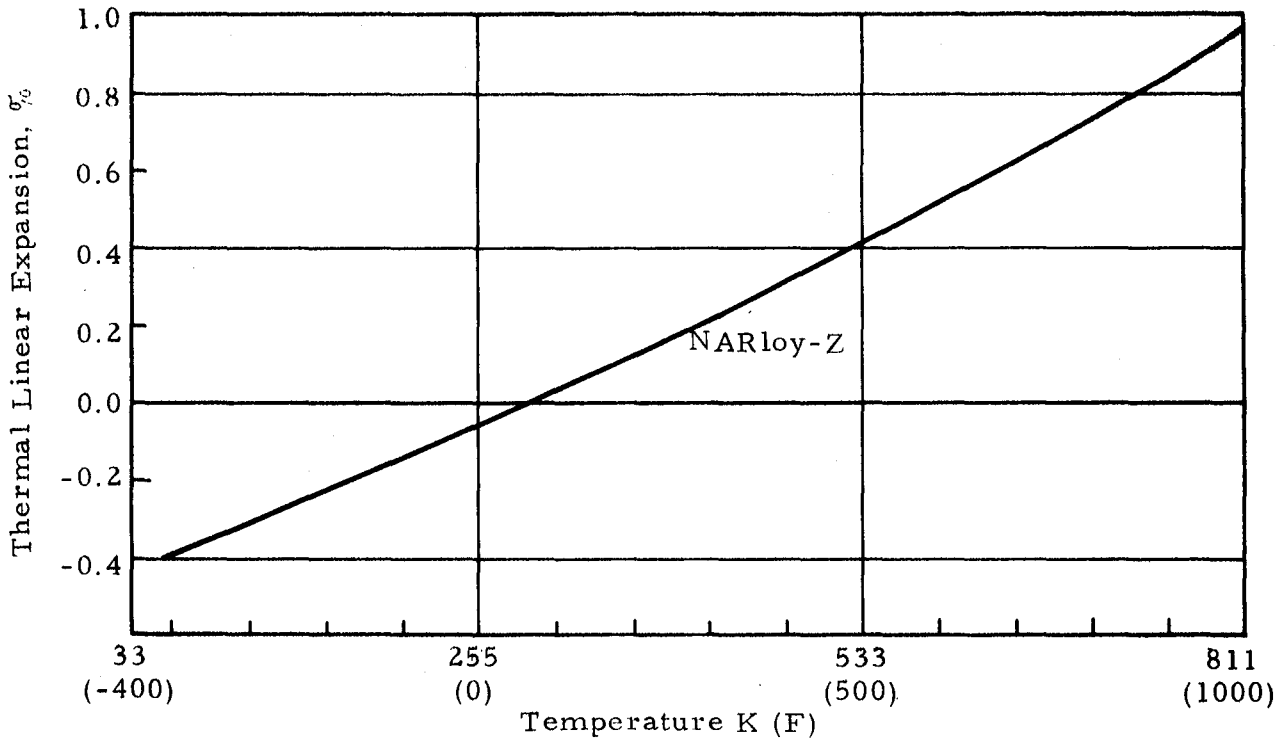

Fig. 2 - Thermal Linear Expansion vs Temperature for NARloy-Z

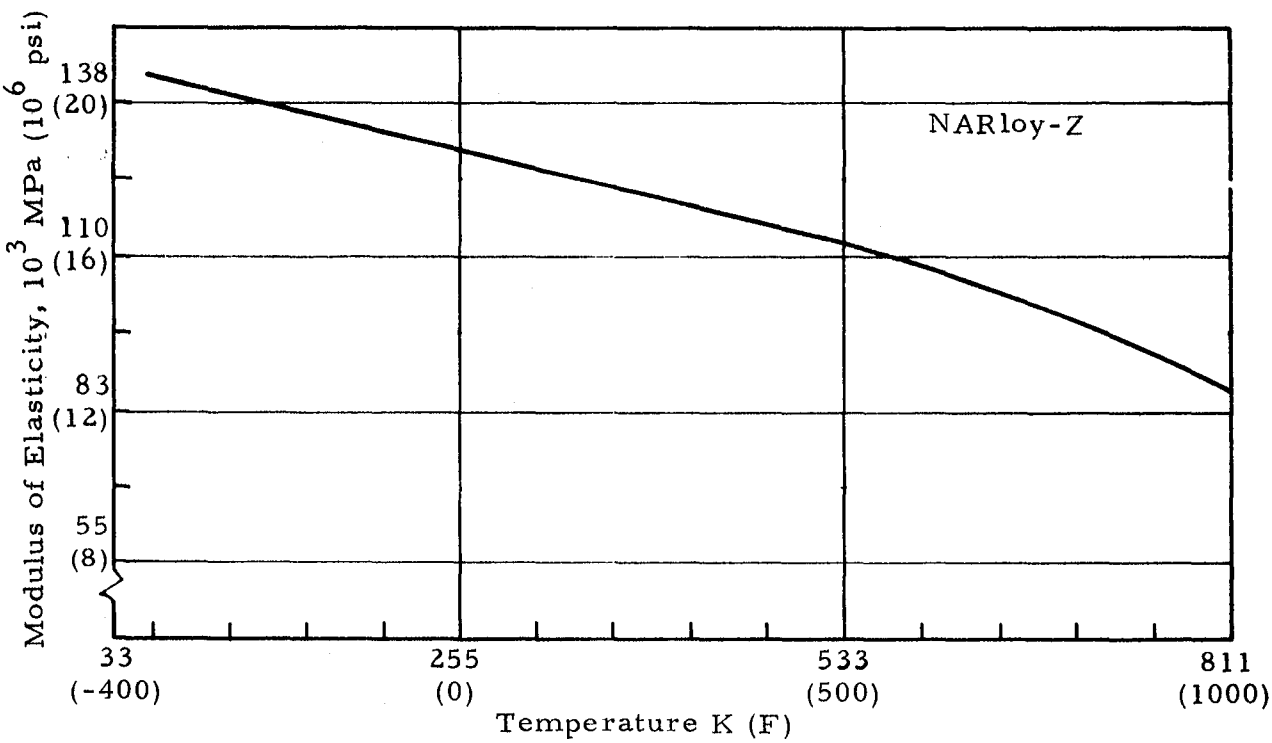

Fig. 3 - Modulus of Elasticity vs Temperature for NARloy-Z

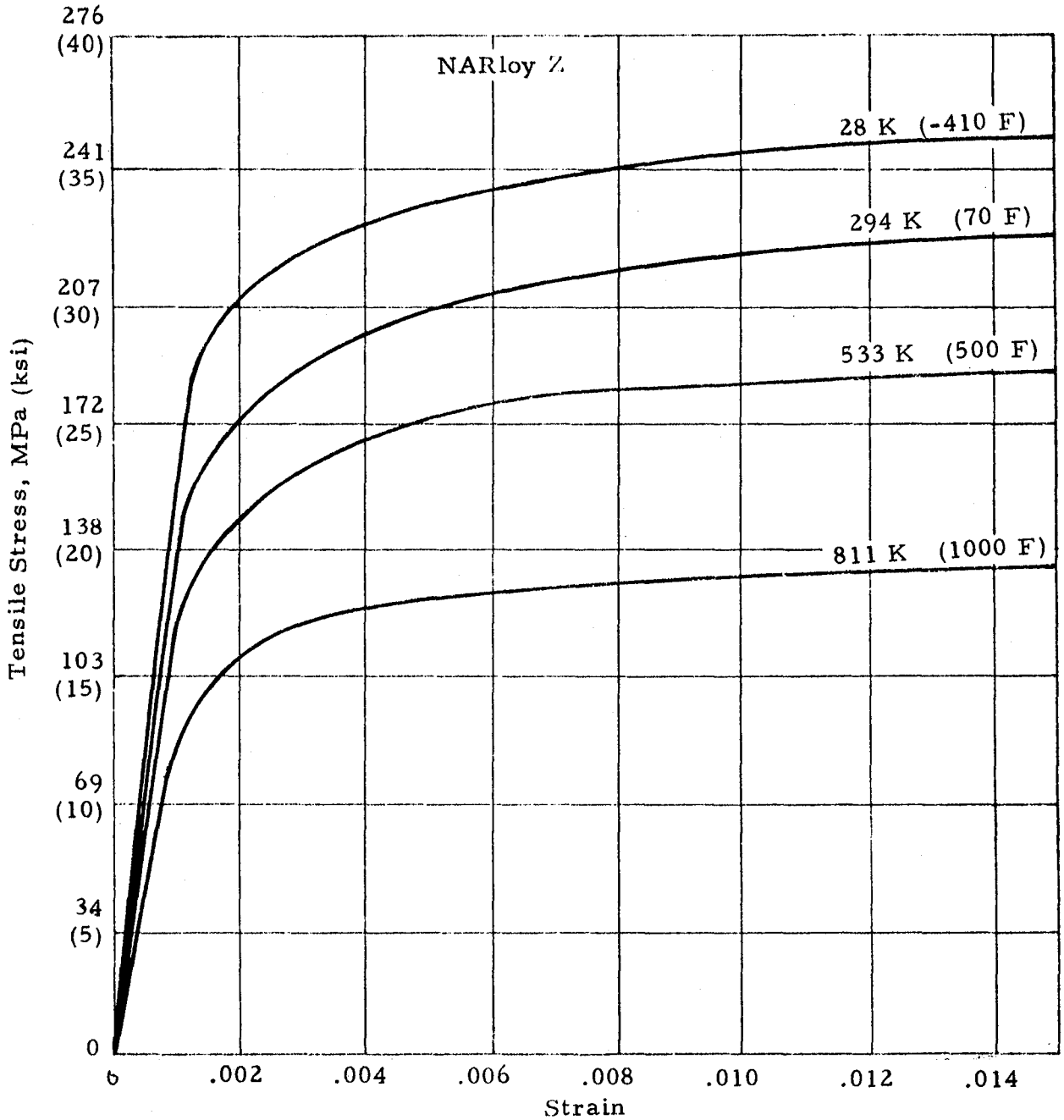

Fig. 4 - Typical Stress-Strain Curves for NARloy-Z

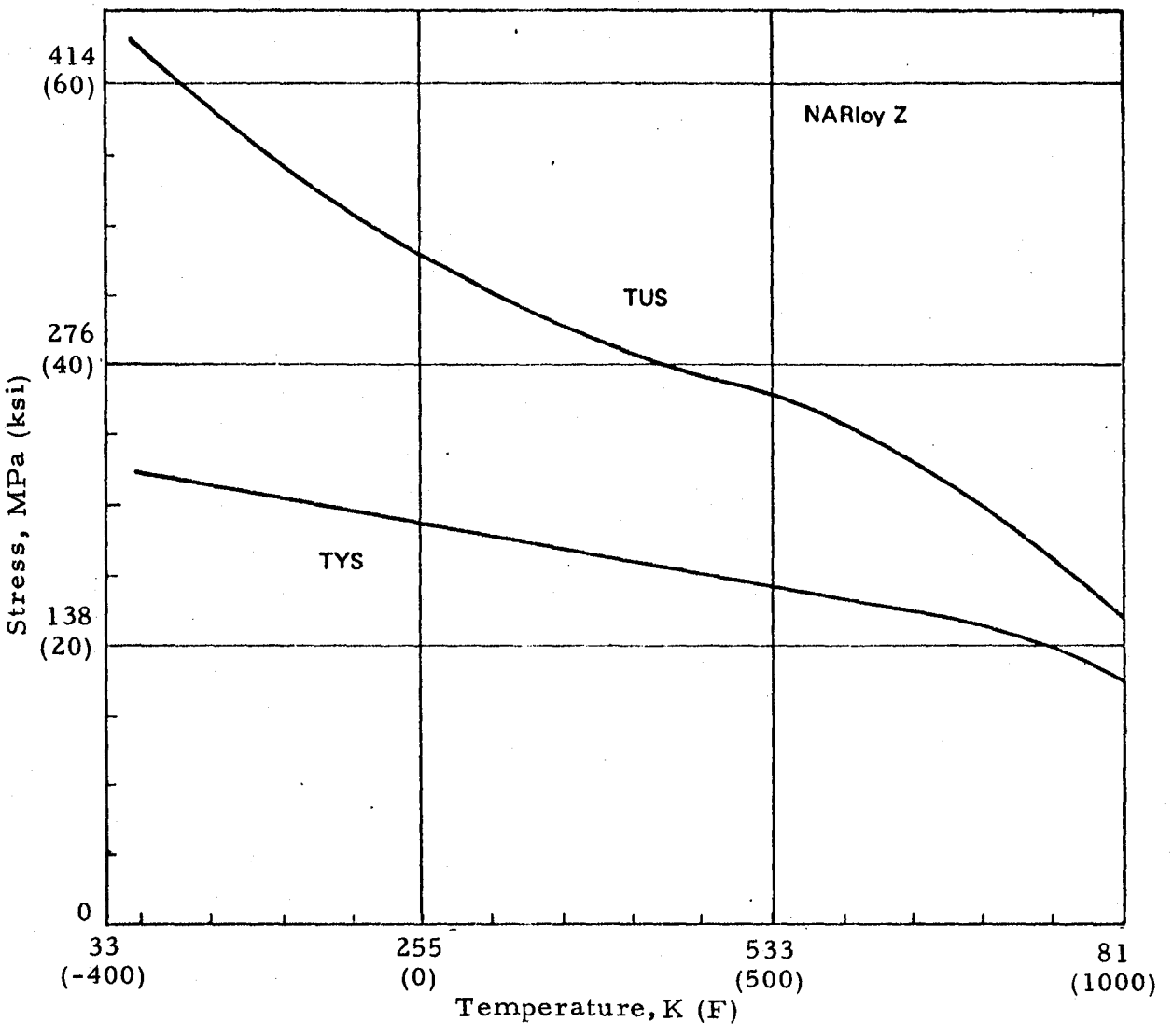

Fig. 5 - Tensile Strength vs Temperature for NARloy-Z

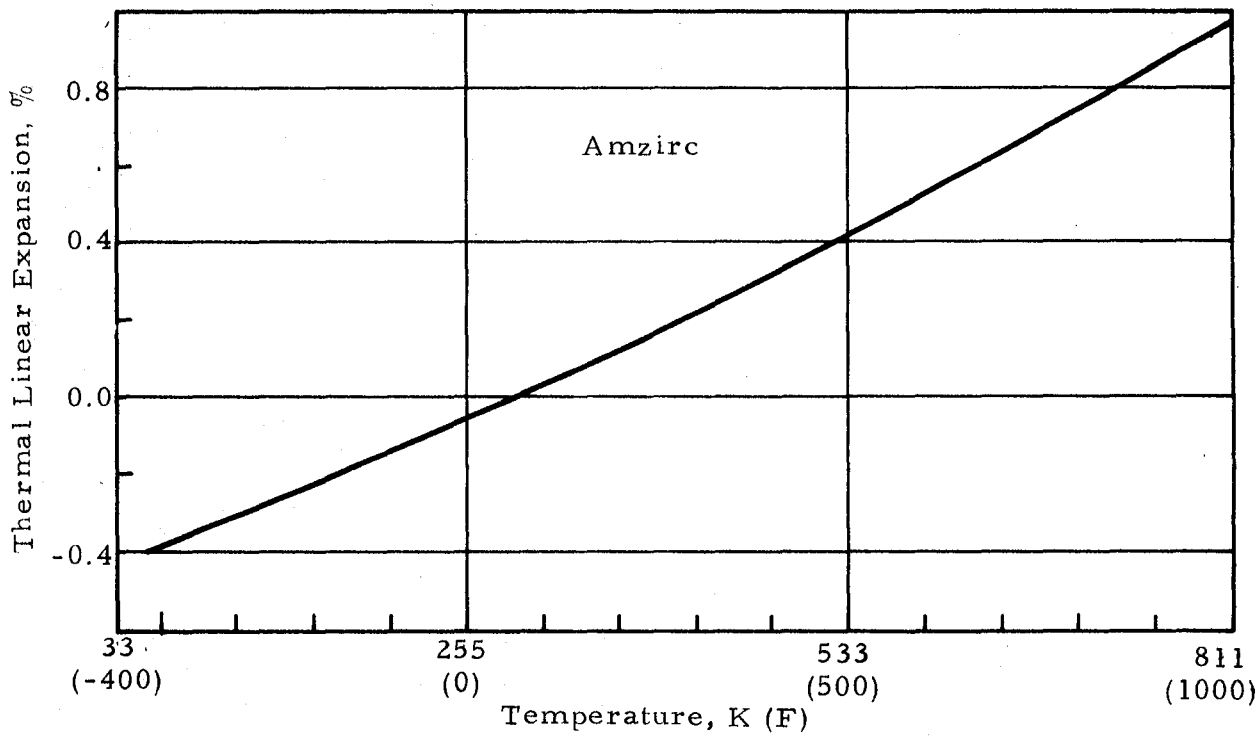

Fig. 6 - Thermal Linear Expansion vs Temperature for Amzirc

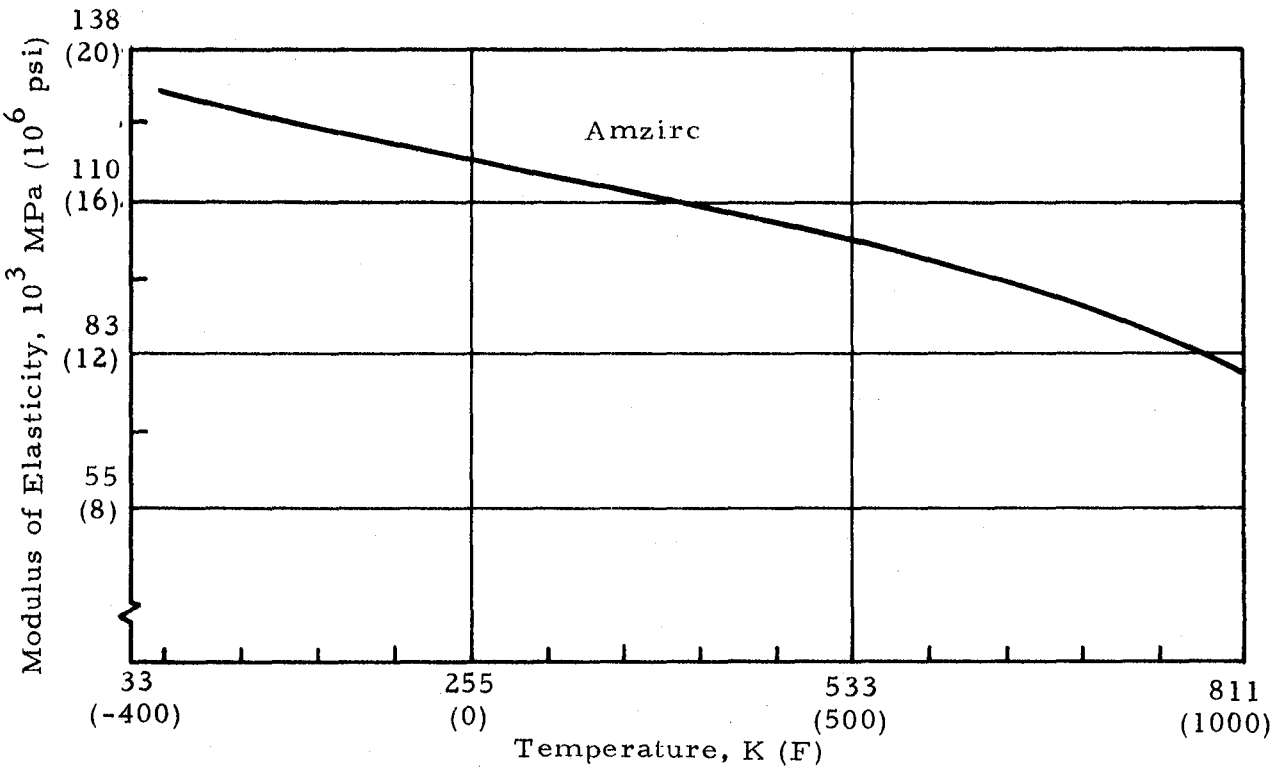

Fig. 7 - Modulus of Elasticity vs Temperature for Amzirc

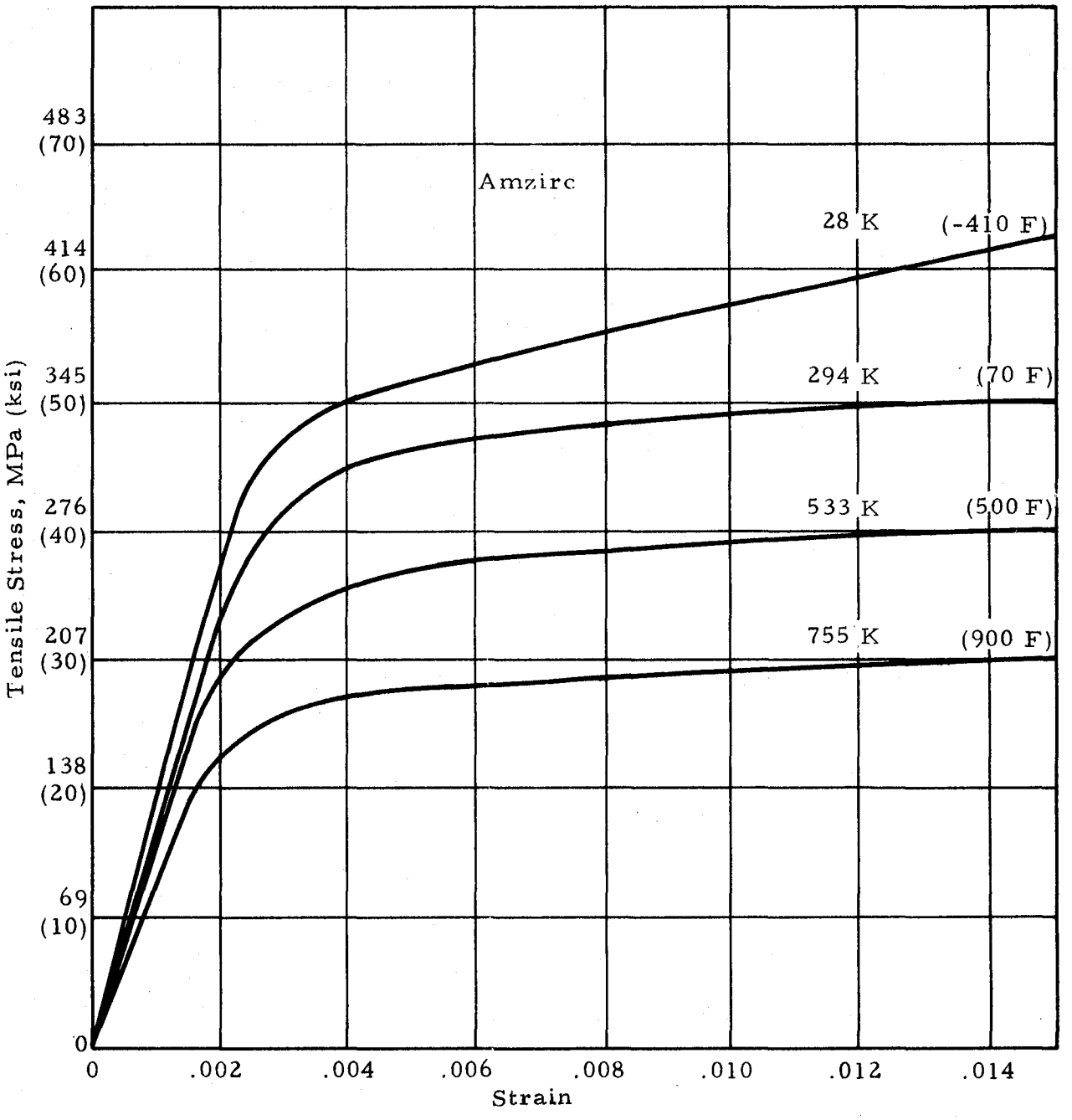

Fig. 8 - Typical Tensile Stress-Strain Curves for Amzirc-Half Hard Condition

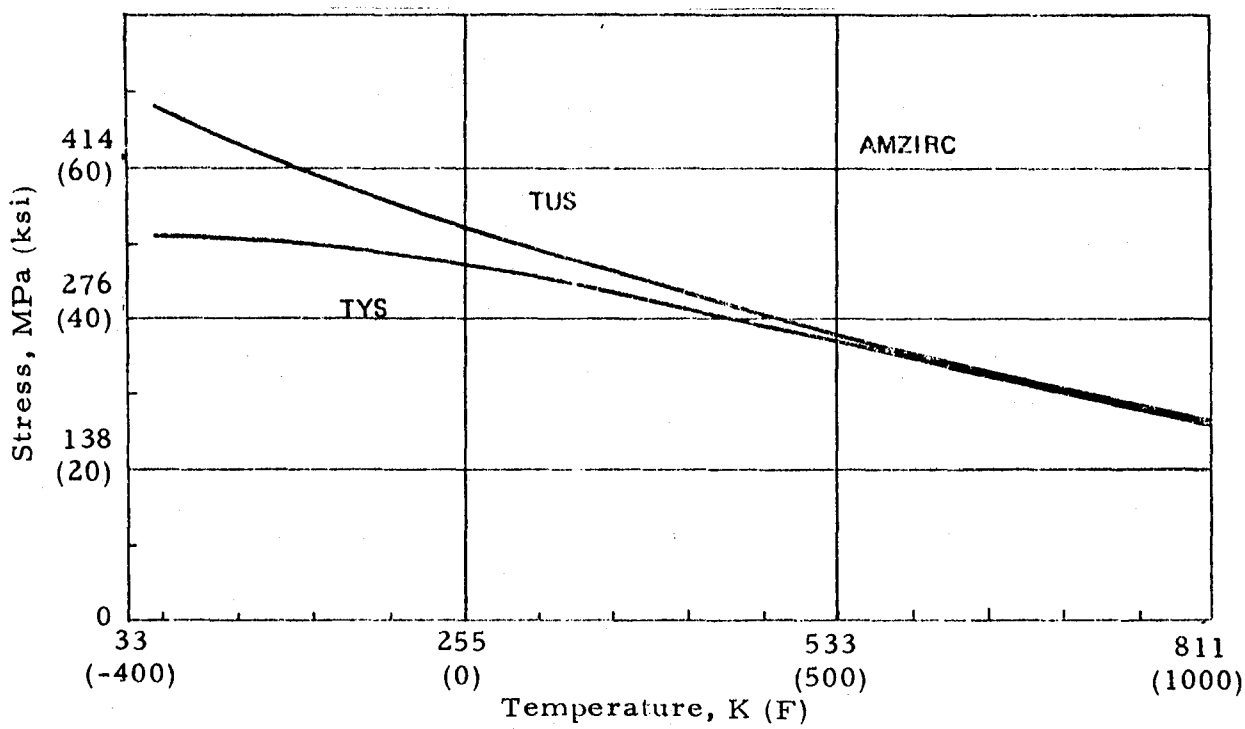

Fig. 9 - Tensile Strength vs Temperature for Amzirc – Half Hard

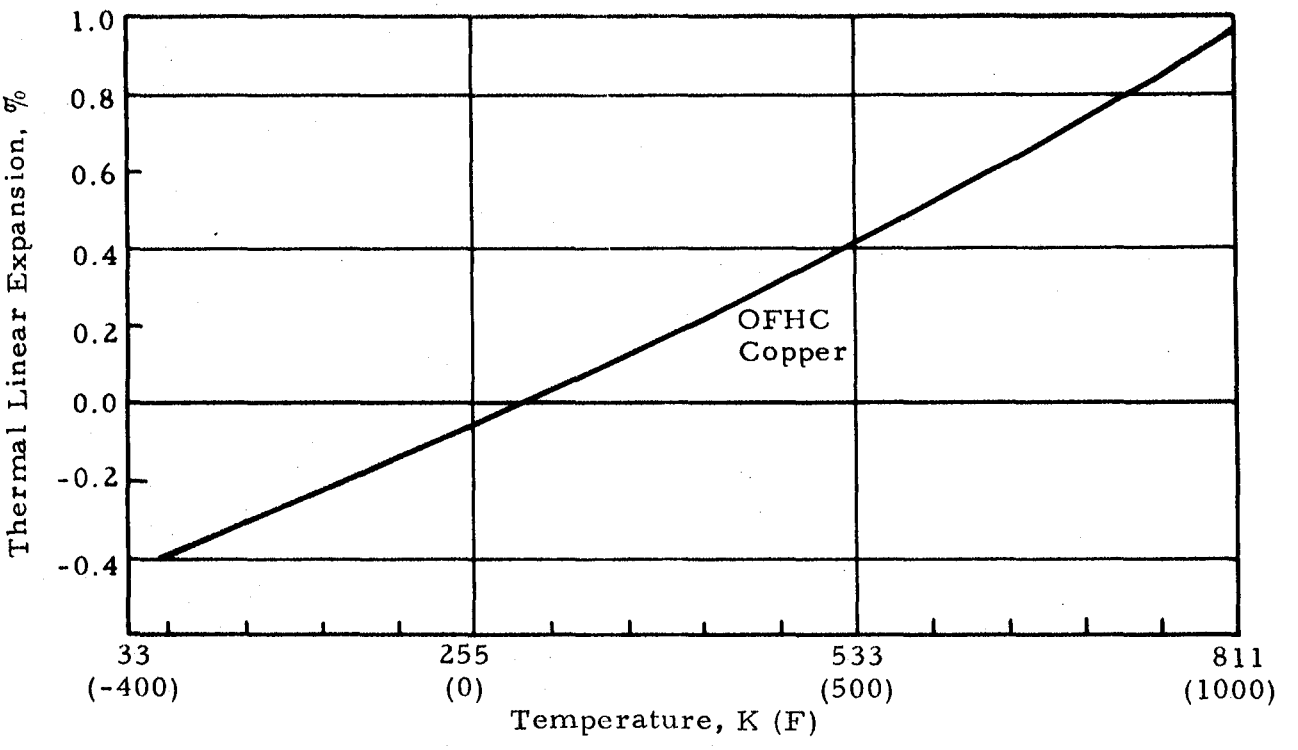

Fig. 10 - Thermal Linear Expansion vs Temperature for OFHC Copper

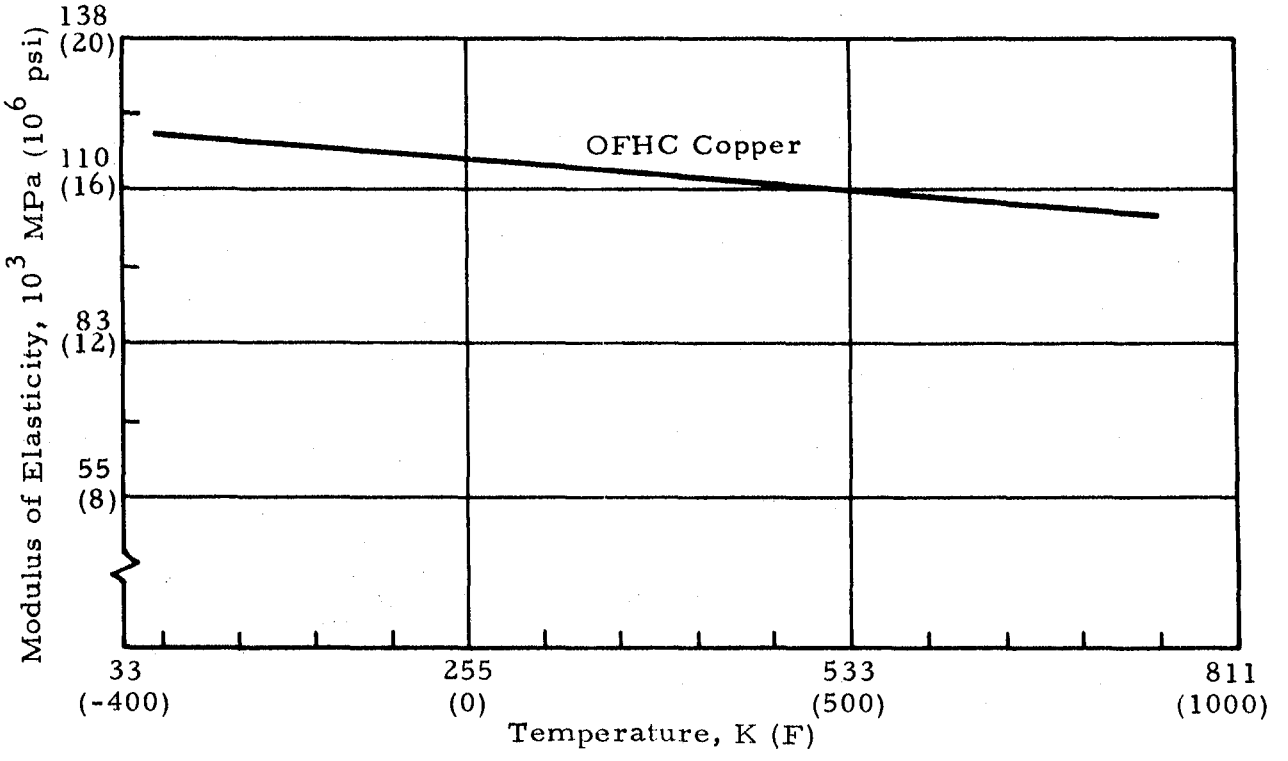

Fig. 11 - Modulus of Elasticity vs Temperature for OFHC Copper

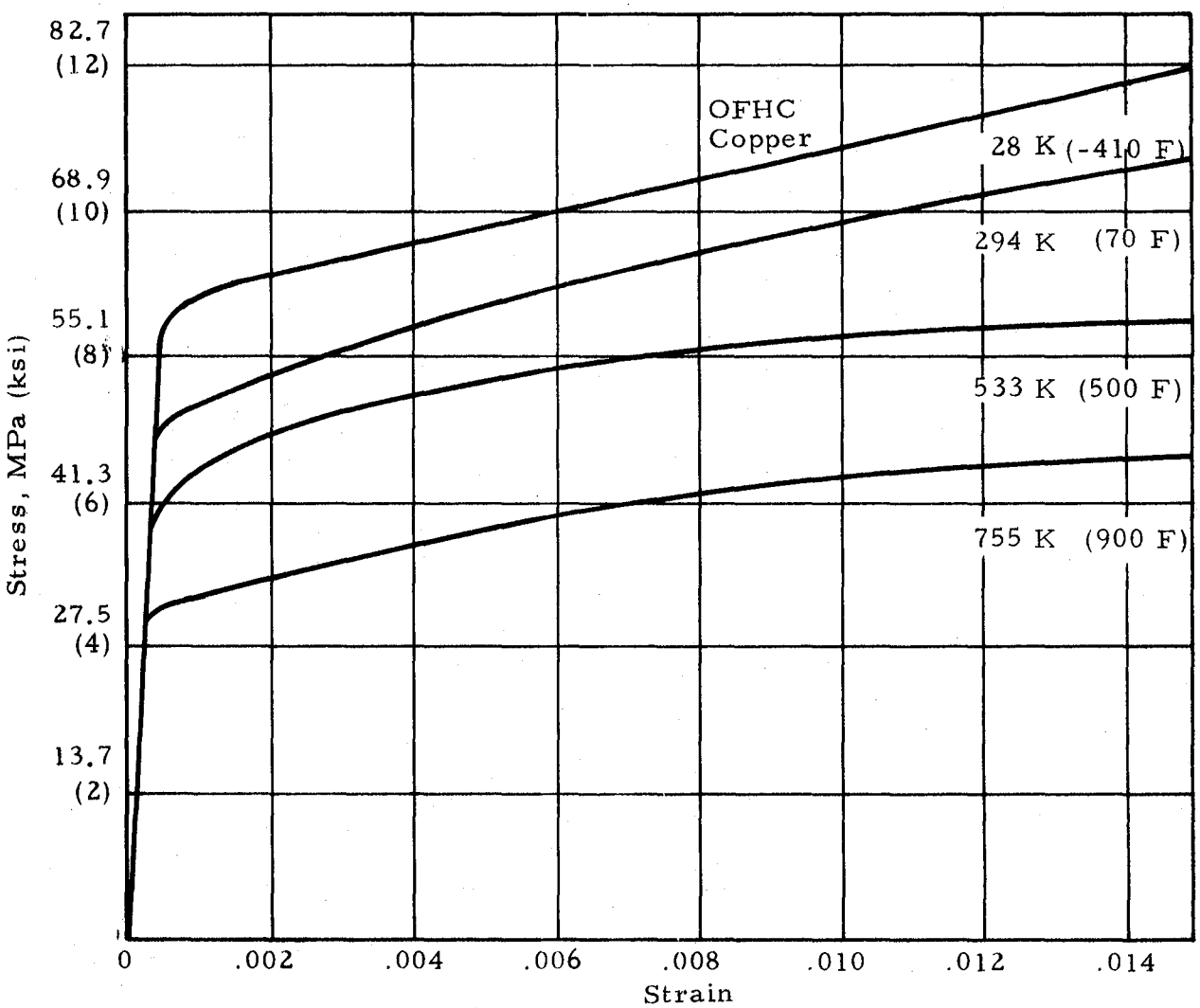

Fig. 12 - Typical Stress-Strain Curves for OFHC Copper Annealed Condition

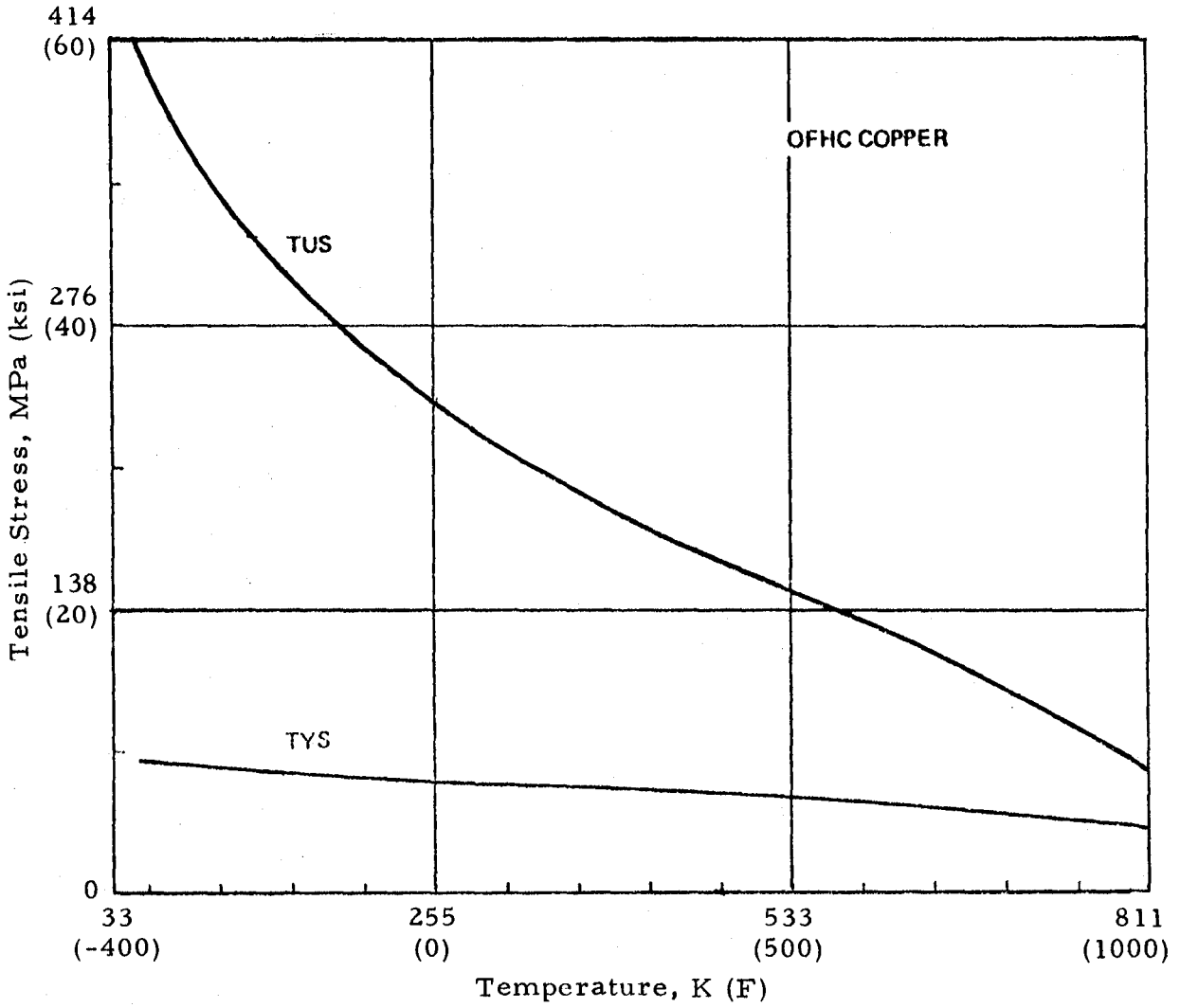

Fig. 13 - Tensile Strength vs Temperature for OFHC Copper Annealed Condition

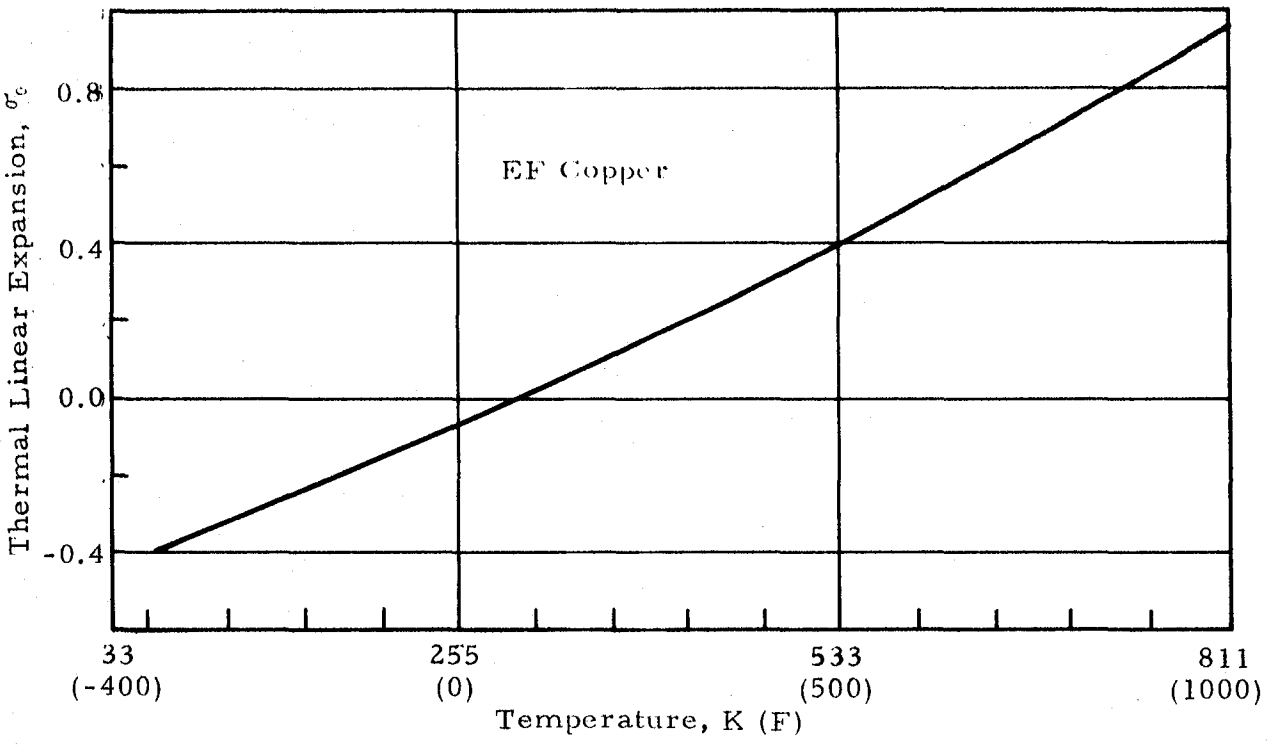

Fig. 14 - Thermal Linear Expansion vs Temperature for Electroformed Copper

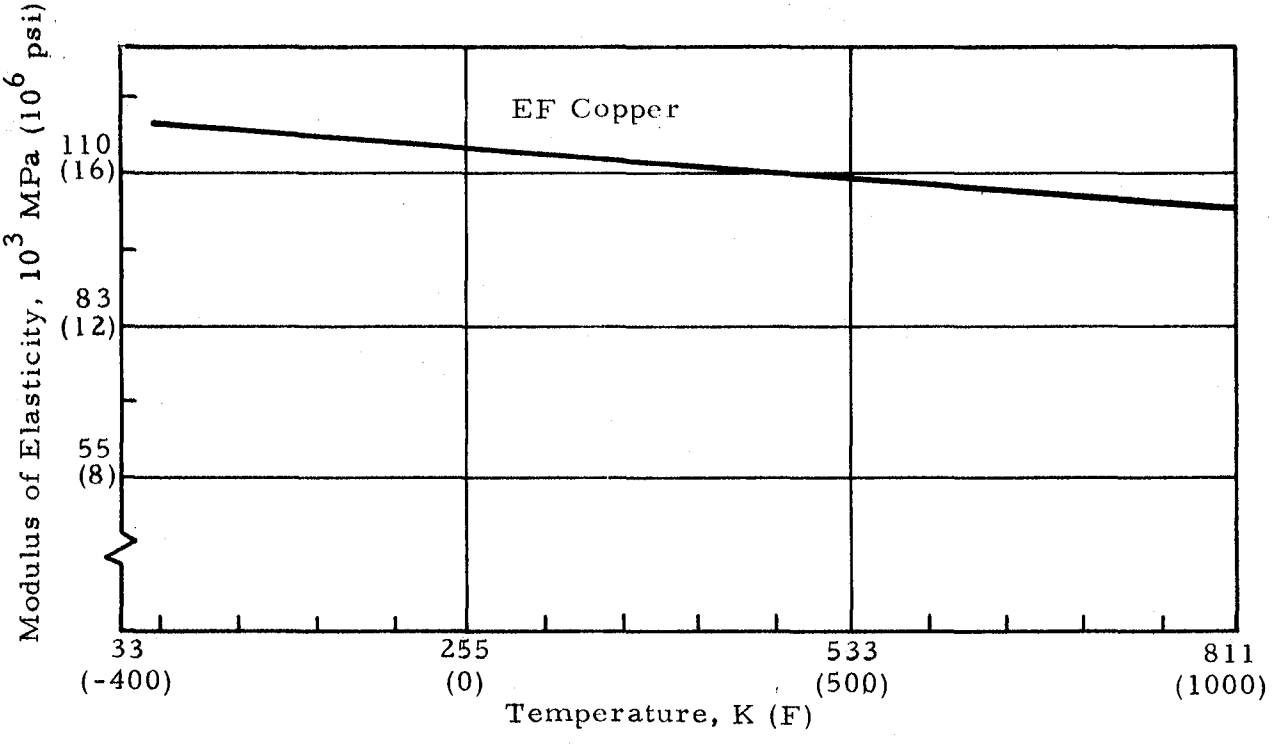

Fig. 15 - Modulus of Elasticity vs Temperature for Electroformed Copper

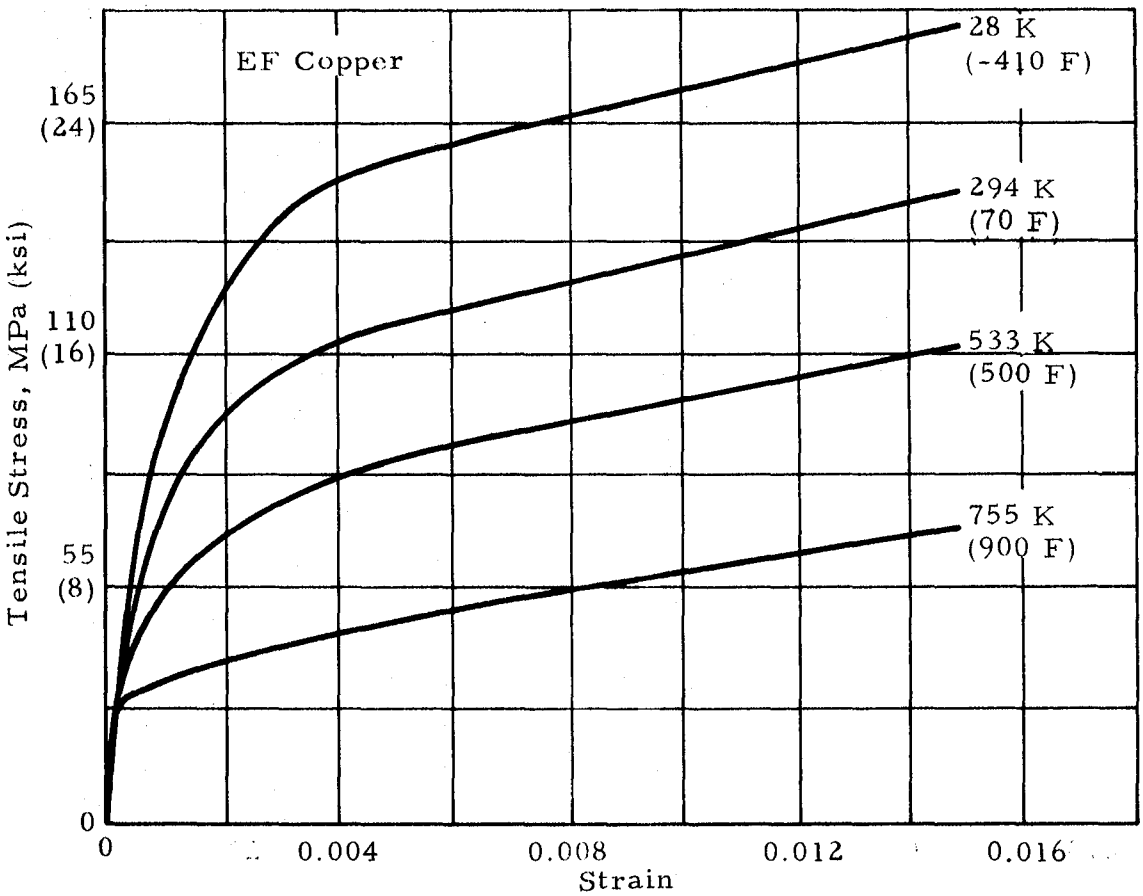

Fig. 16 - Typical Stress-Strain Curves for Electroformed Copper — as-Formed Condition

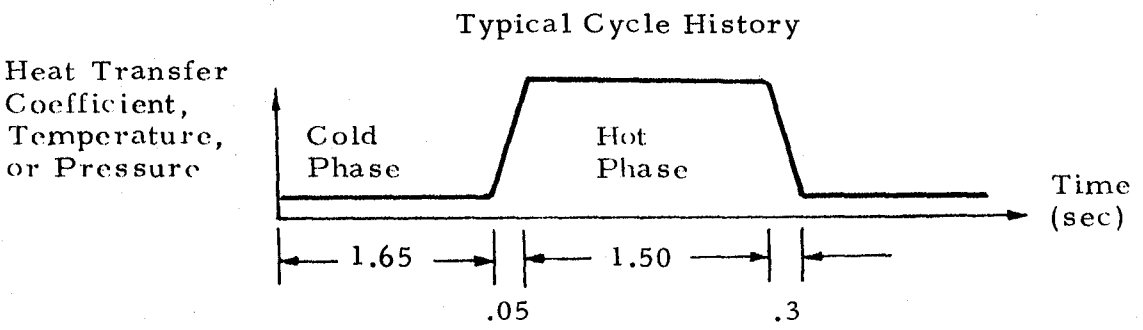

Cycle Phase	Cold	Hot
Hot Gas Side Heat Transfer Coefficient W/cm^2-K (Btu/in^2-sec-R)	0.0	2.02 (0.00685)
Hot Gas Side Adiabatic Wall Temperature K (R)	278 (500)	3364 (6055)
Hot Gas Side Wall Pressure kPa (psia)	96.5 (14.0)	2780 (403)
Coolant Side Heat Transfer Coefficient W/cm^2-K (Btu/in^2-sec-R)	10.2 (.0345)	4.83 (0.0164)
Coolant Side Bulk Temperature K (R)	28 (50)	50 (90)
Coolant Side Wall Pressure kPa (psia)	5100 (740)	6550 (950)

Fig. 17 - Boundary Conditions for Baseline Cyclic Structural Temperatures and Pressures

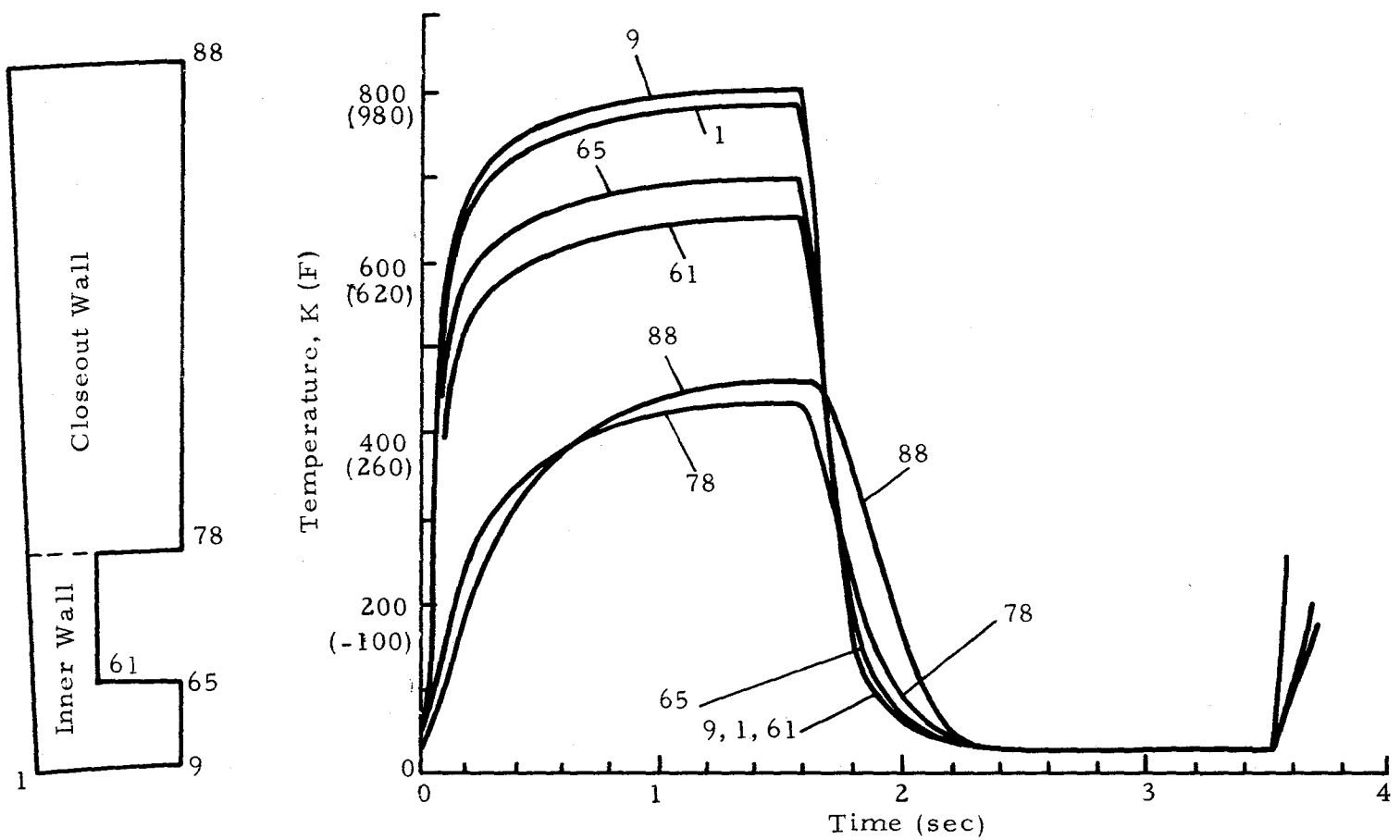

Fig. 18 - Temperature Histories for Baseline Boundary Conditions

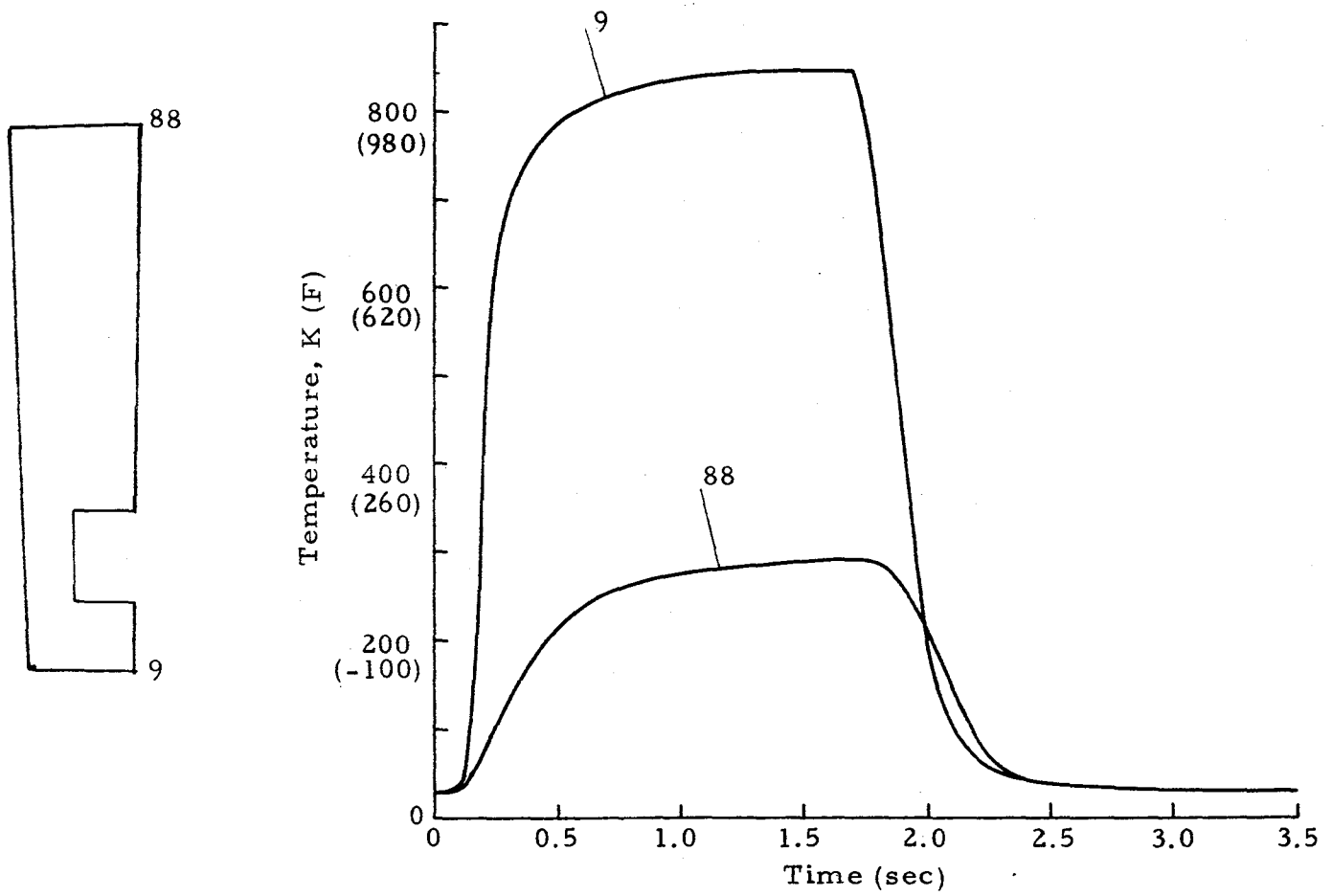

Fig. 19 - SN 34 Temperature Histories

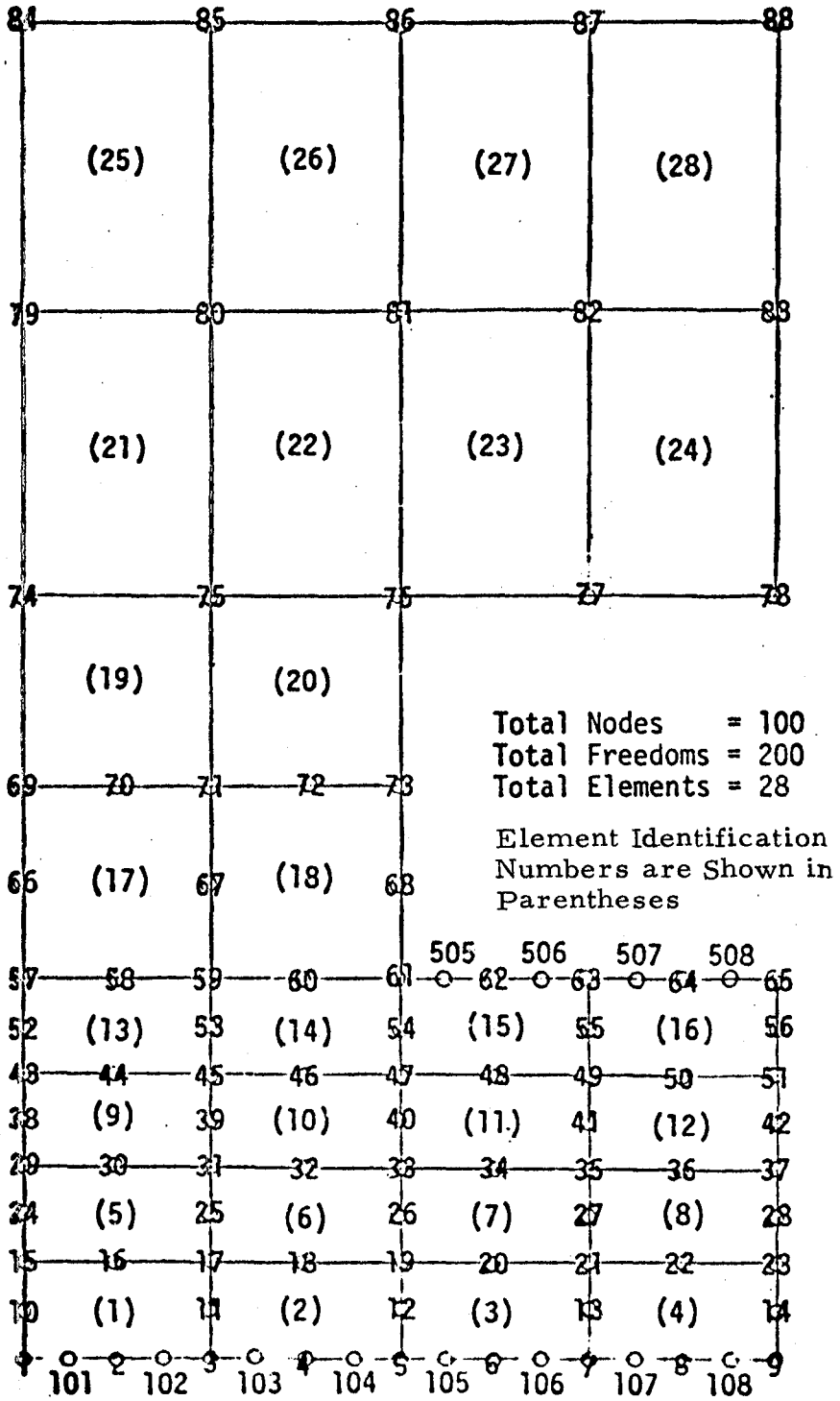

Fig. 20 - Schematic of BOPACE Model Showing Node and Element Identification Numbers

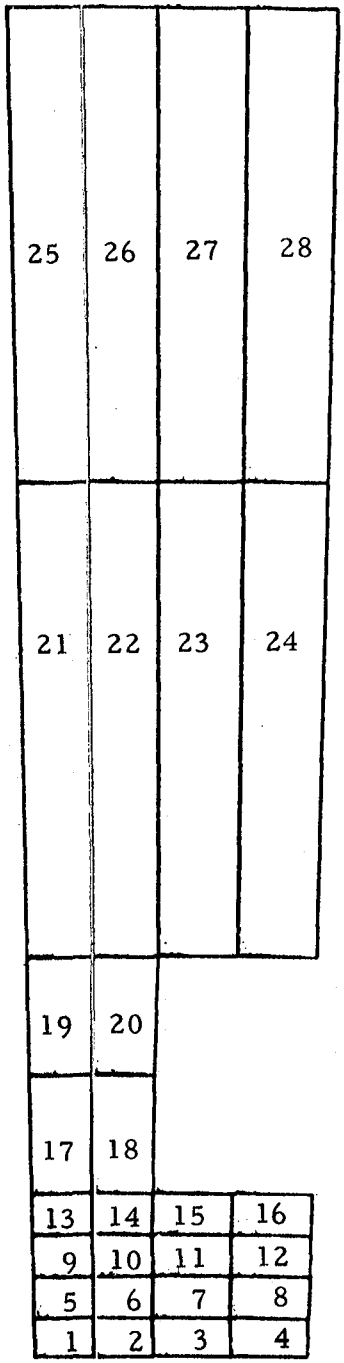

Total Nodes = 100

Total Freedoms = 200

Total Elements = 28

Fig. 21 - Computer Plot of Undeformed Thrust Chamber Model

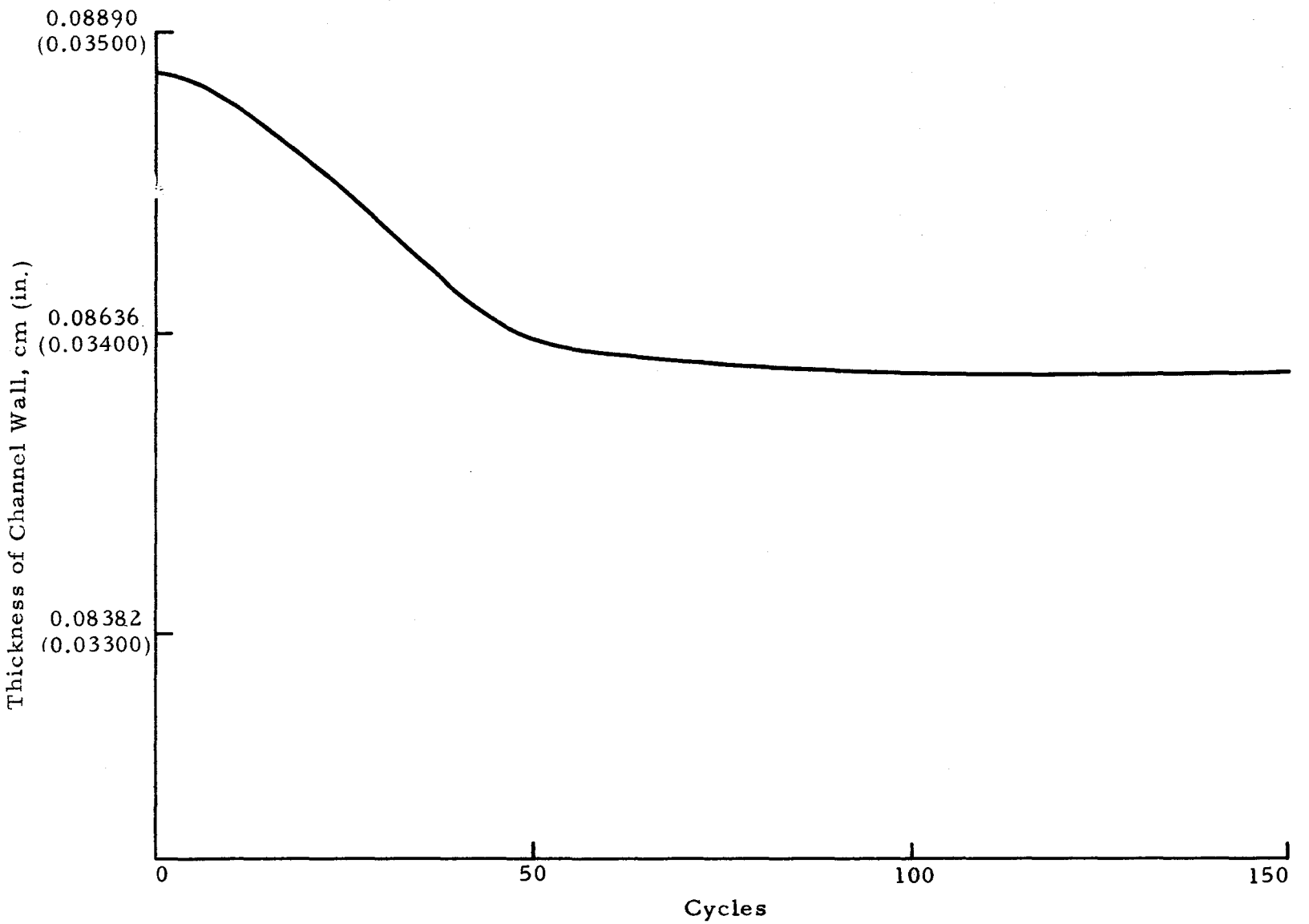

Fig. 22 - Amzirc Channel Wall Thickness at Channel Centerline, Baseline Load Cycle

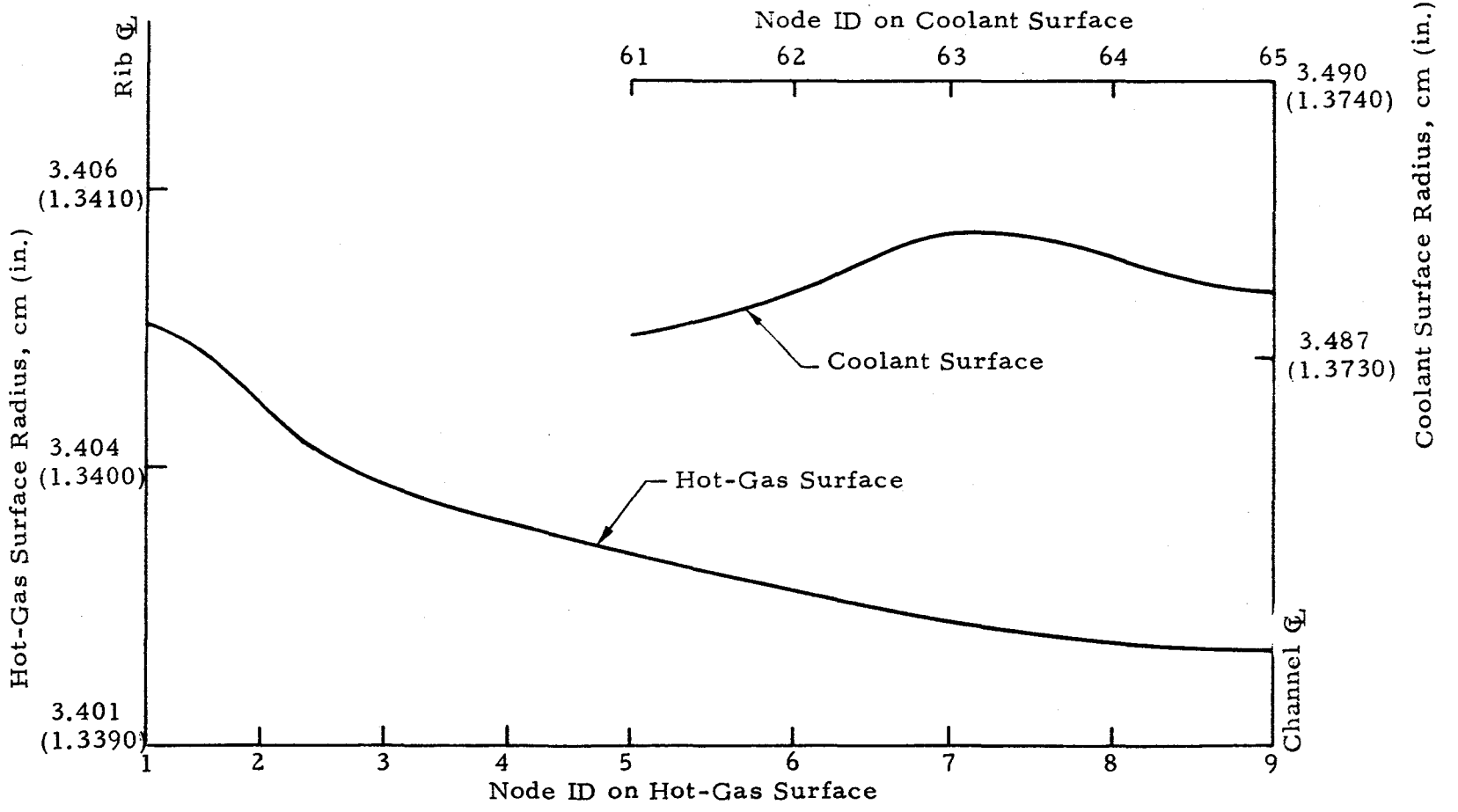

Fig. 23 - Hot-Gas and Coolant Surface Profiles of Amzirc/EFCU Chamber After 100 Baseline Cycles

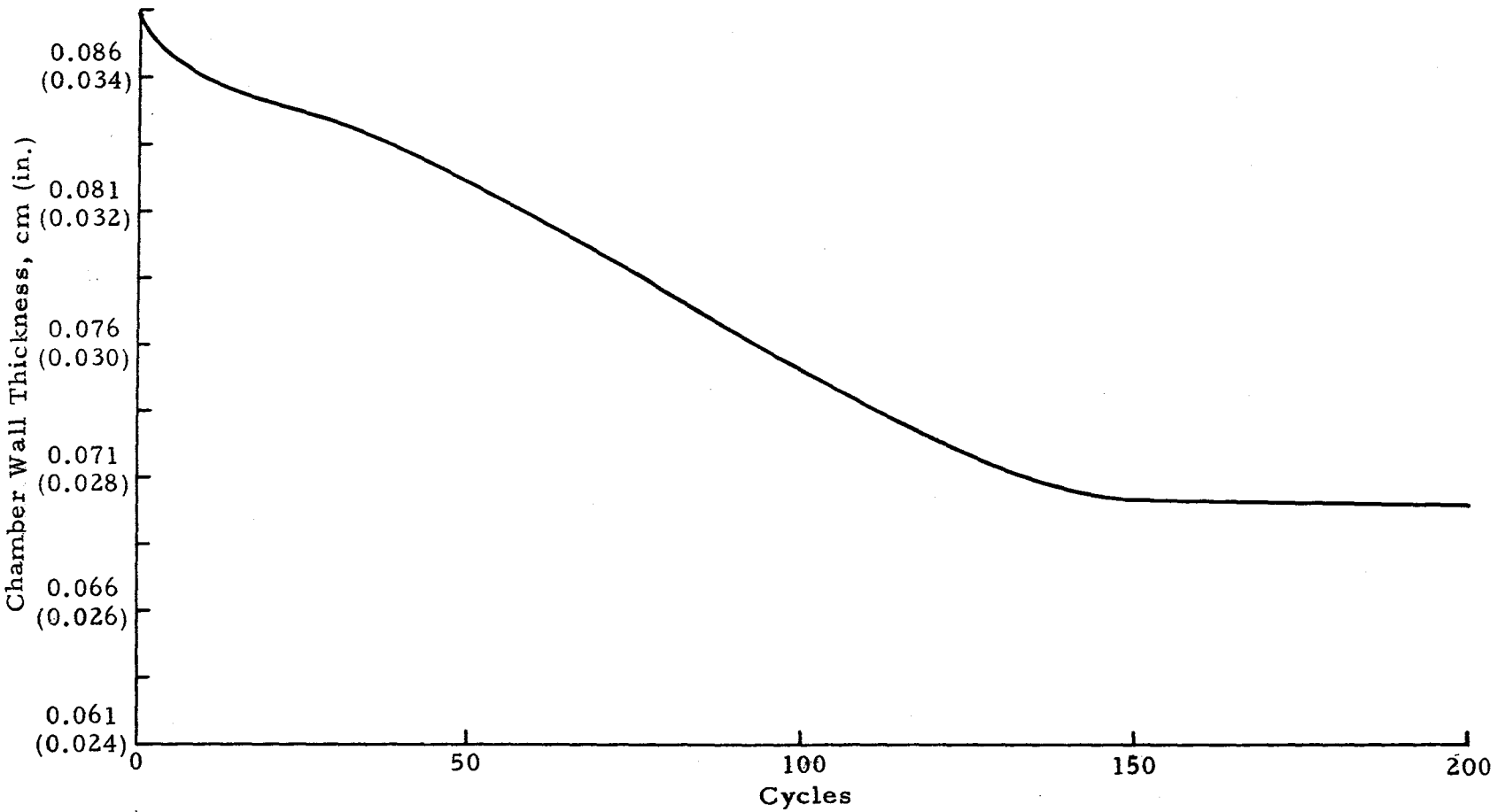

Fig. 24 - OFHC Chamber Wall Thickness at Channel Centerline, Baseline Load Cycle

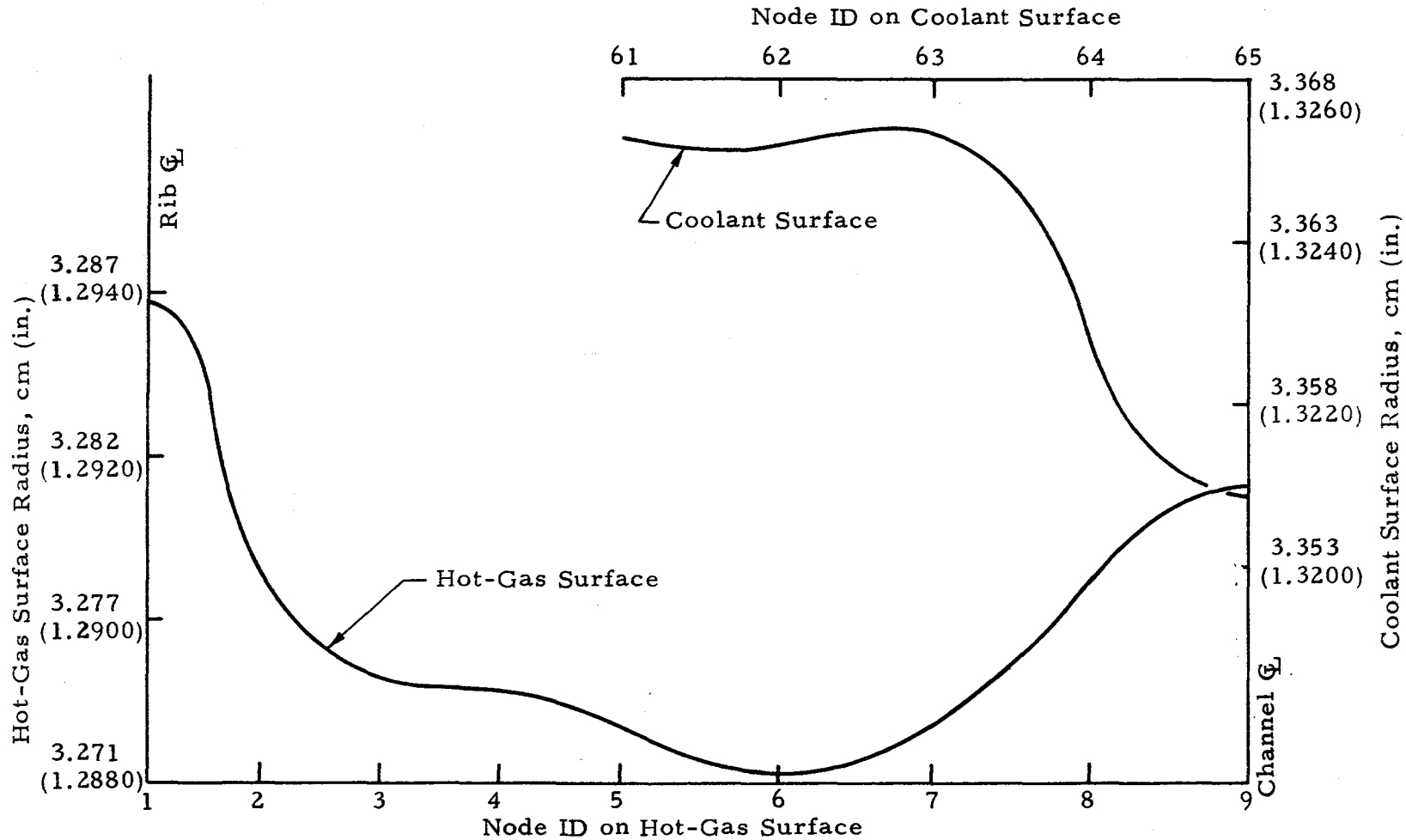

Fig. 25 - Hot-Gas and Coolant Surface Profiles of OFHC/EFCU Chamber After 100 Baseline Cycles

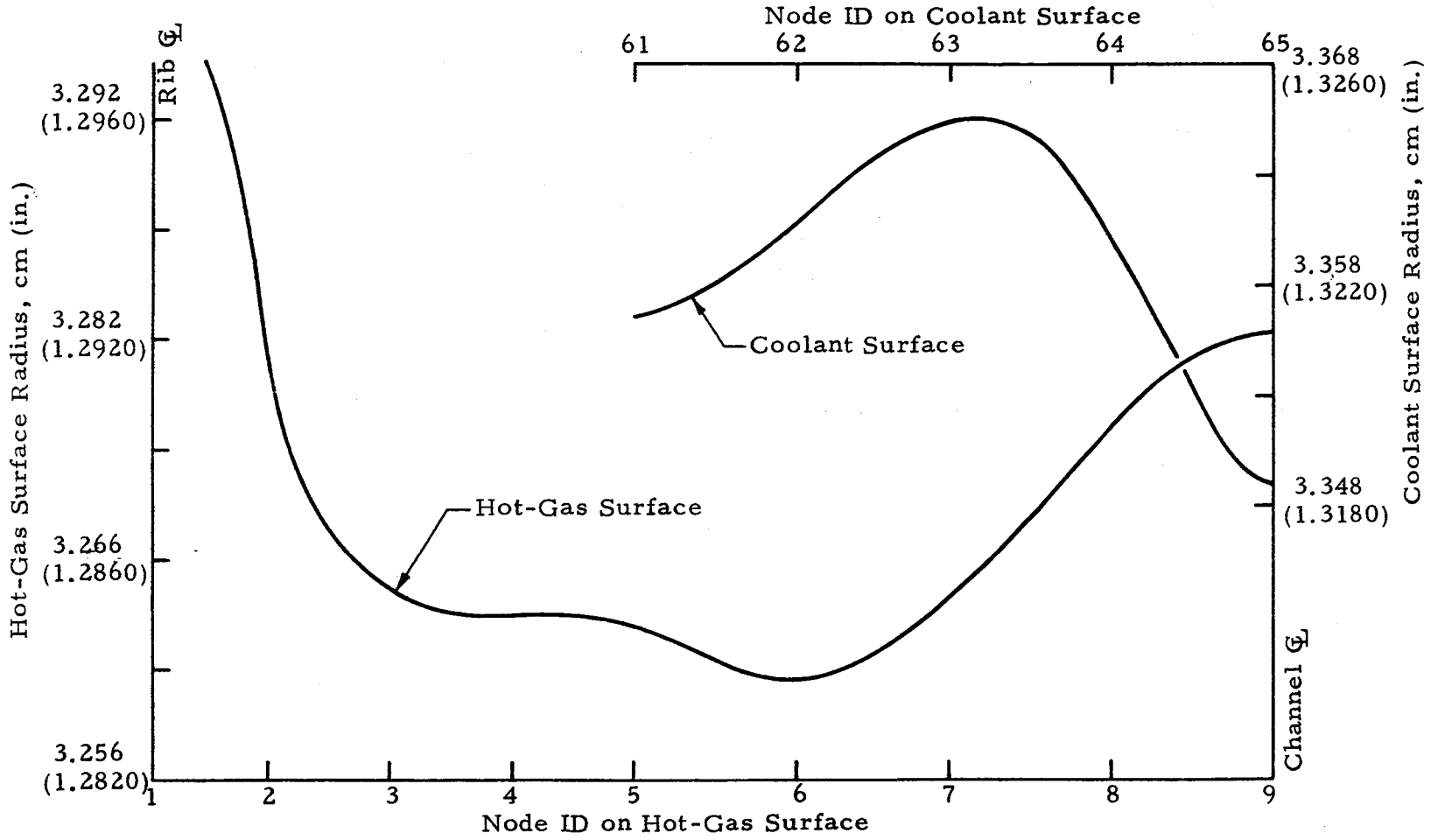

Fig. 26 - Hot-Gas and Coolant Surface Profiles of OFHC/EFCU Chamber After 200 Baseline Cycles

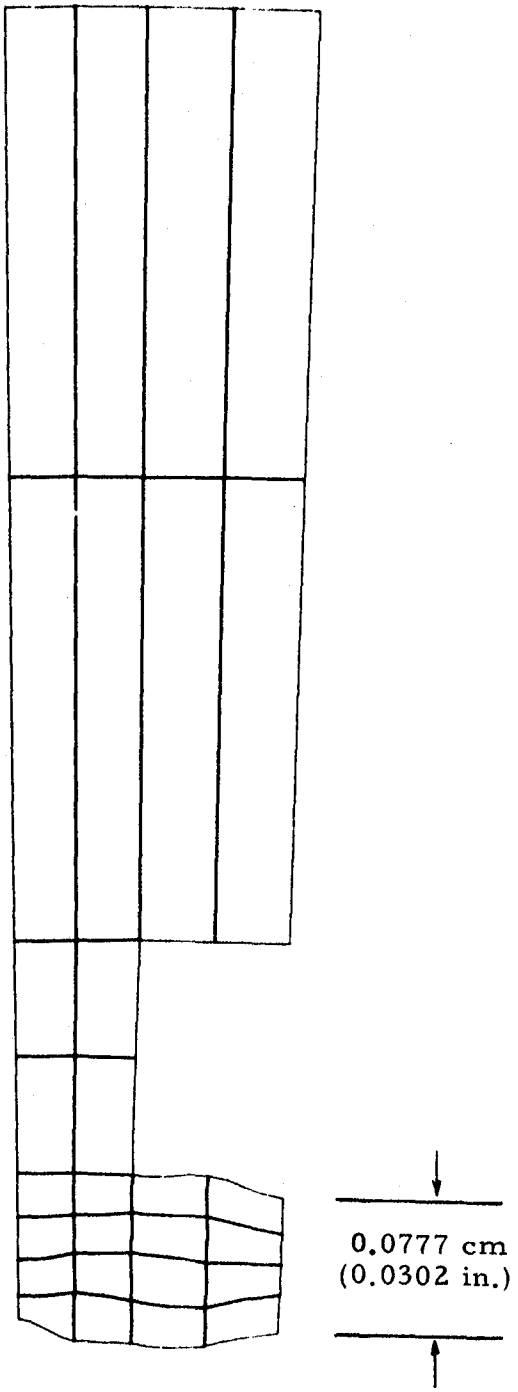

Fig. 27 - Computer Plot of Predicted Configuration of OFHC/EFCU Chamber after 100 Baseline Load Cycles

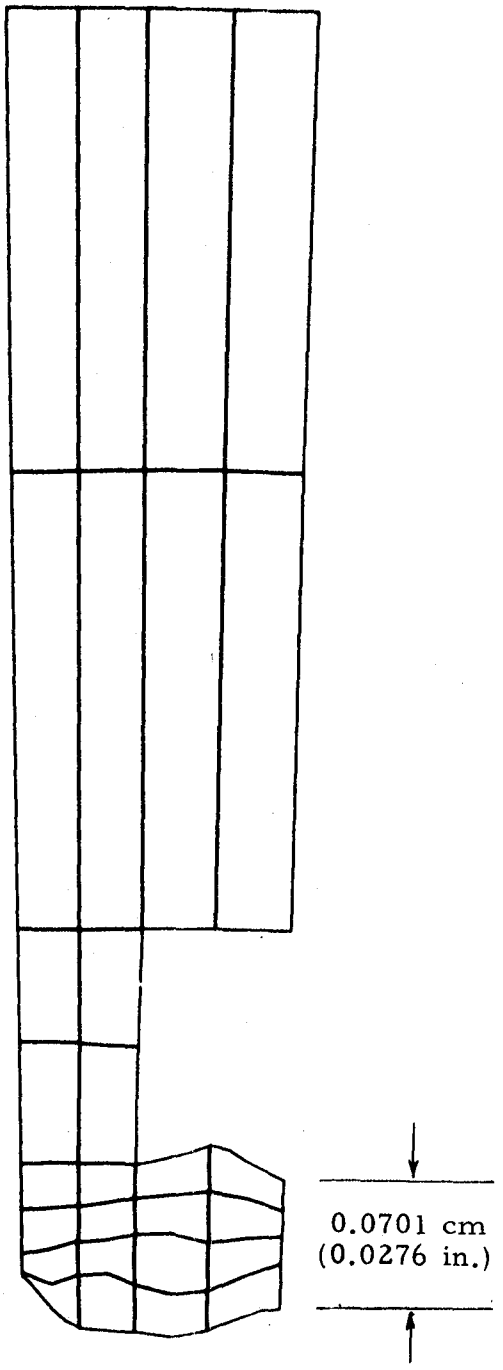

Fig. 28 - Computer Plot of Predicted Configuration of OFHC/EFCU Chamber after 200 Baseline Load Cycles

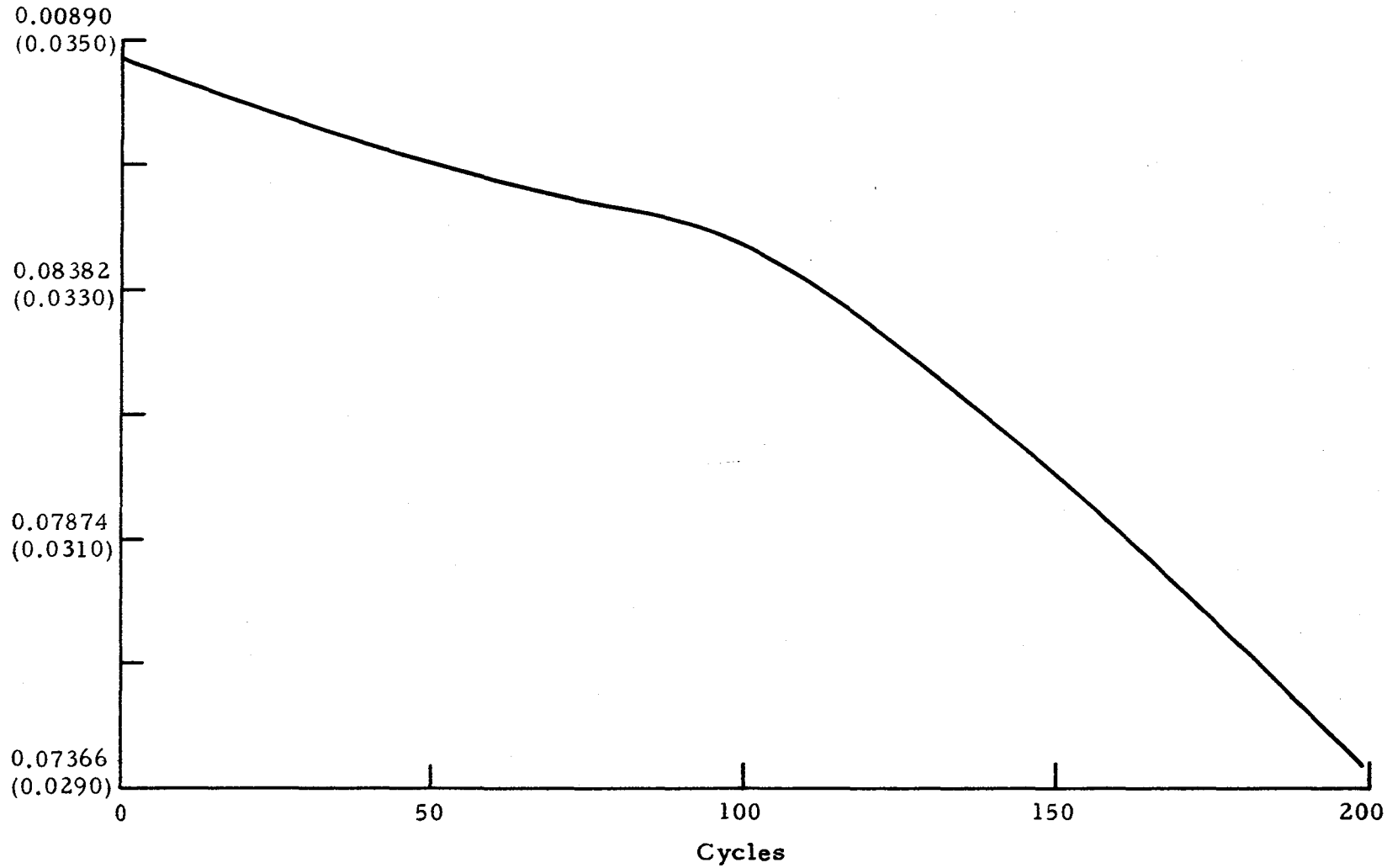

Fig. 29 - OFHC Chamber Wall Thickness at Channel Centerline, SN 34 Load Cycle

Parameter	Heating Phase (t = 0 to 1.70 sec)	Cooling Phase (t = 1.70 to 3.50 sec)
OFHC Density	8913 kg/m^3	No Change
OFHC Thermal Conductivity	389 W/mK	No Change
OFHC Specific Heat	419 J/kg K	No Change
EDNi Density	8858 kg/m^3	No Change
EDNi Thermal Conductivity	87 W/mK	No Change
EDNi Specific Heat	167 J/kg K	No Change
Combustion Cham. Gas Temp.	3289 K	283 K
Coolant Passage Gas Temp.	56 K	28 K
Outer Wall Gas Temp.	294 K	294 K
Inner Wall Film Coefficient	831 W/m^2 K	137 W/m^2 K
Coolant Pass. Film Coeff., Inner Wall	1251 W/m^2 K	4018 W/m^2 K
Coolant Pass. Film Coeff., Rib	3250 W/m^2 K	5022 W/m^2 K
Coolant Pass. Film Coeff., Outer Wall	5022 W/m^2 K	5022 W/m^2 K
Outer Wall Film Coeff.	0.176 W/m^2 K	0.176 W/m^2 K

Fig. 30 - Thermal Parameters Used in NASTRAN Two-Dimensional Heat Conduction Analysis of OFHC/EDNi Thrust Chamber

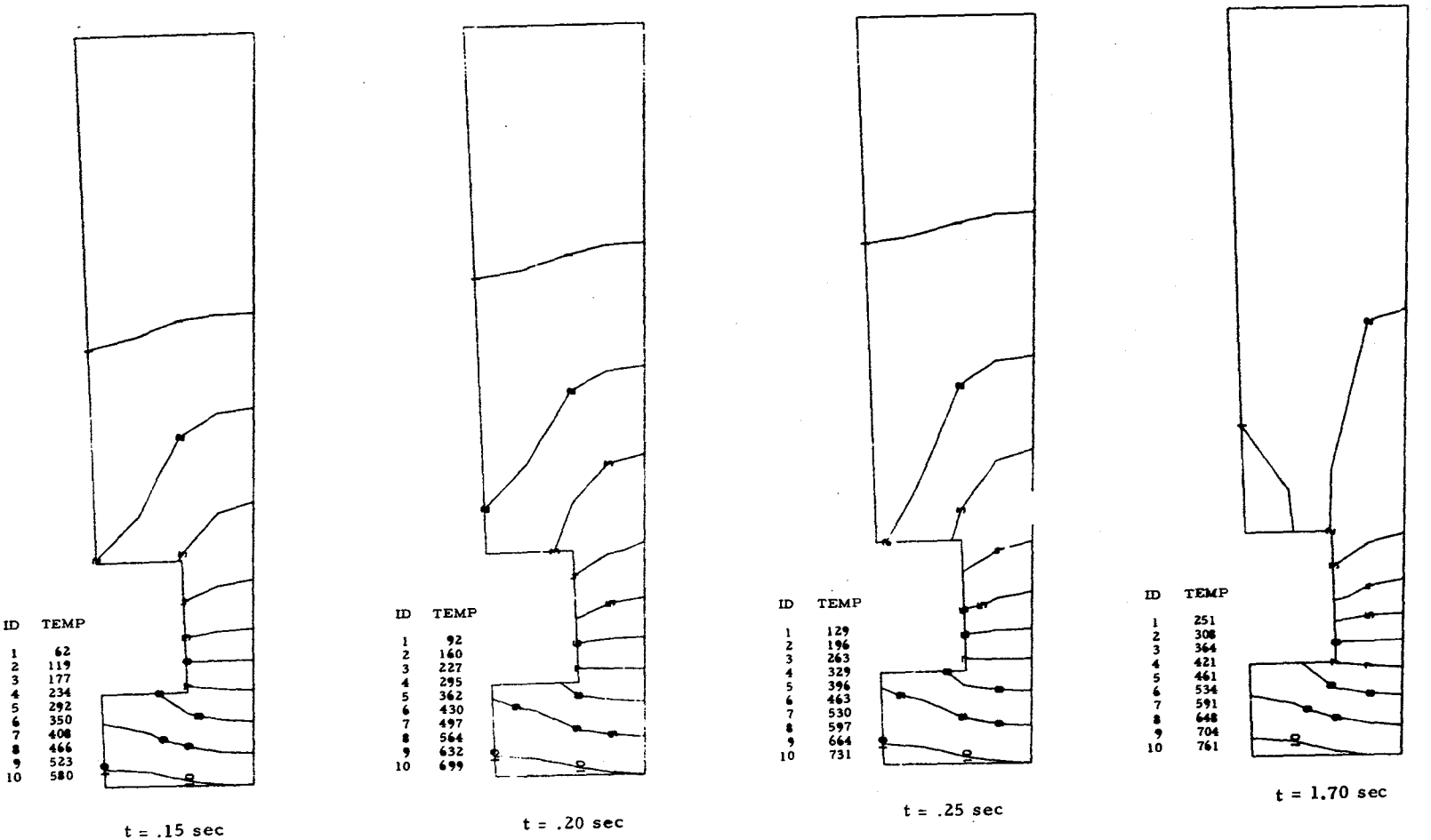

Notes:

1. Initial temperature = 28 K uniform.
2. All temperatures are degrees Kelvin.

Fig. 31 - OFHC/EDNi Temperatures for SN 34 Heating Phase (t = 0 to 1.70 sec)

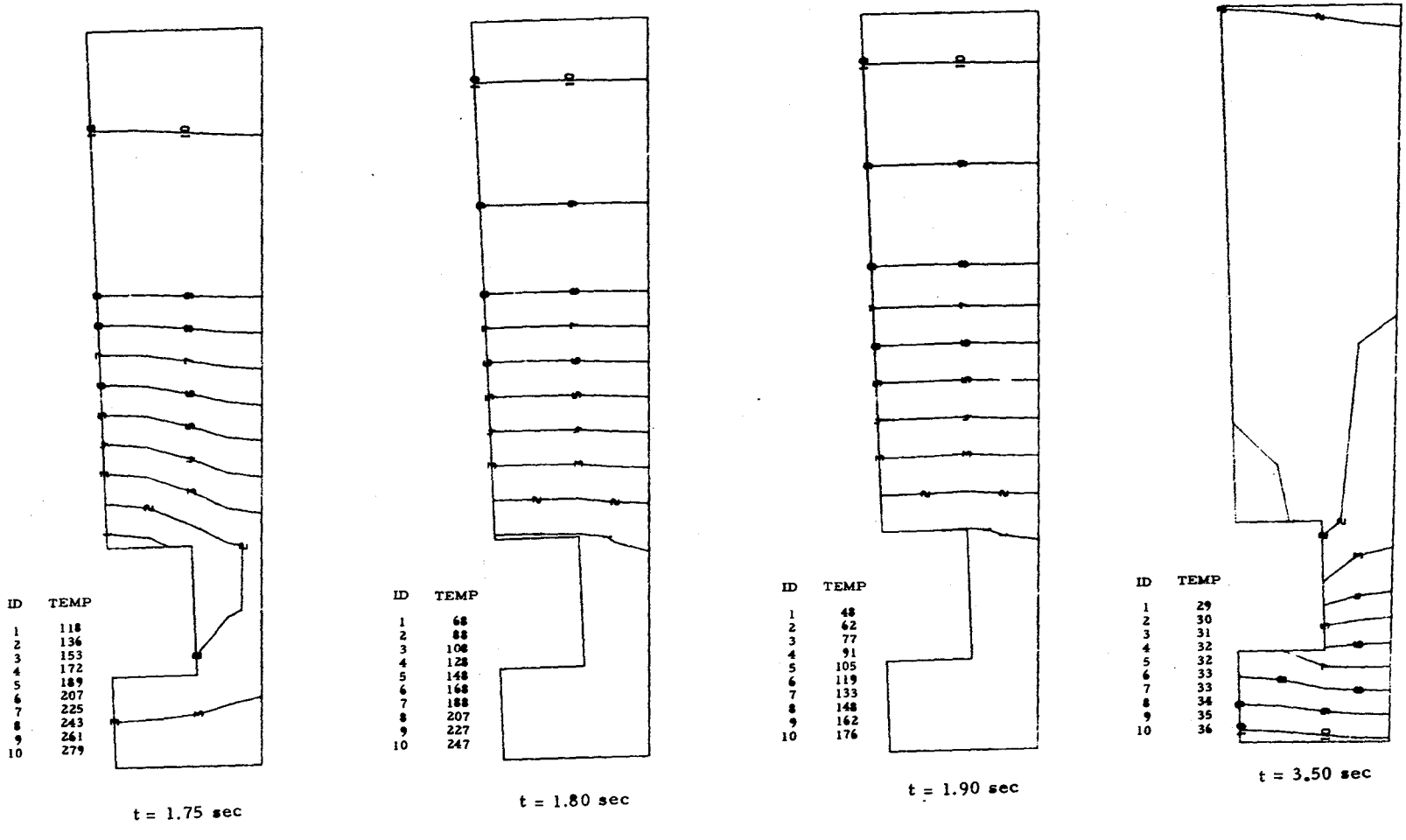

Note: All temperatures are degrees Kelvin.

Fig. 32 - OFHC/EDNi Temperatures for SN 34 Cooling Phase (t = 1.70 to 3.50 sec)

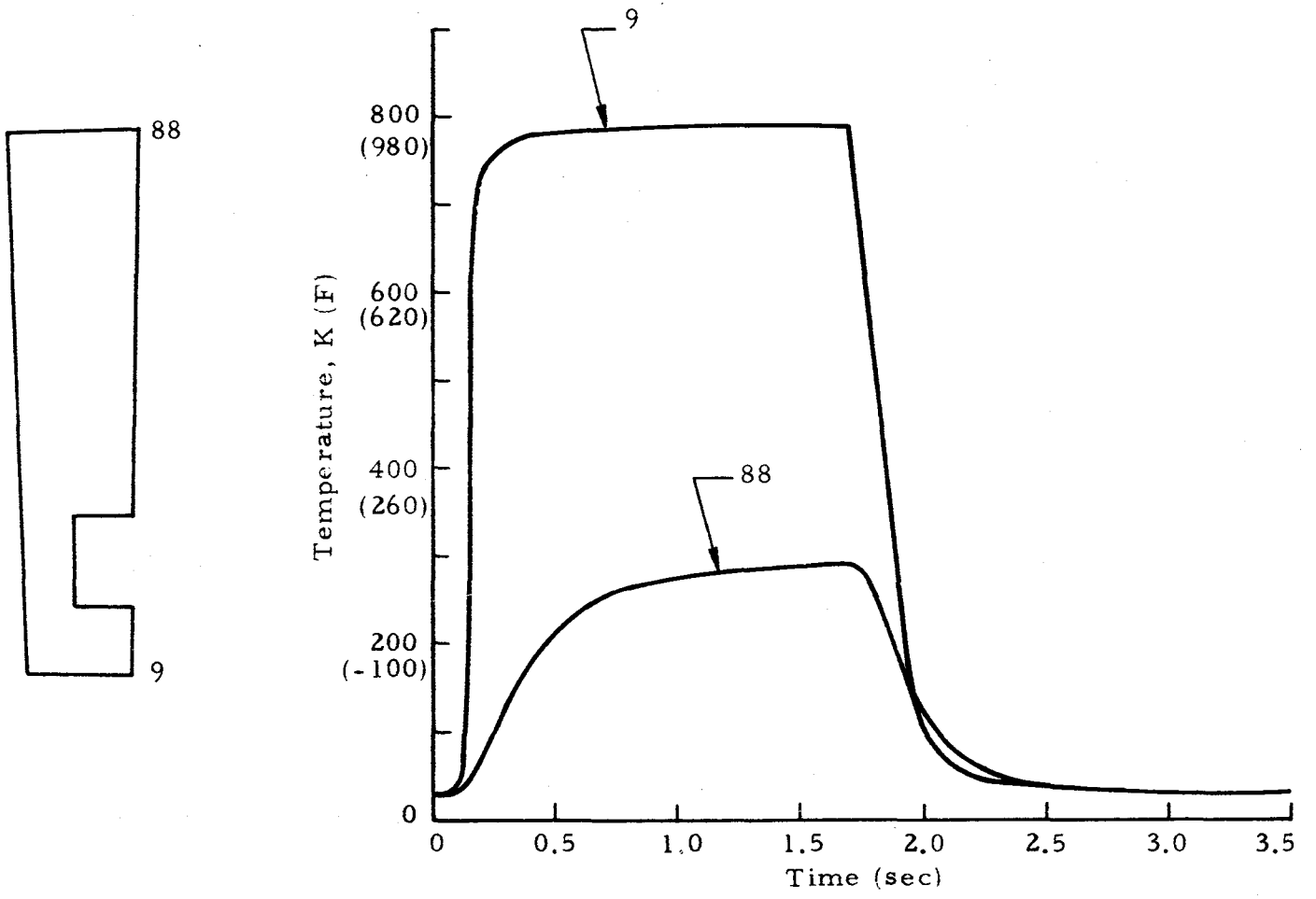

Fig. 33 - OFHC/EDNi Temperature Histories

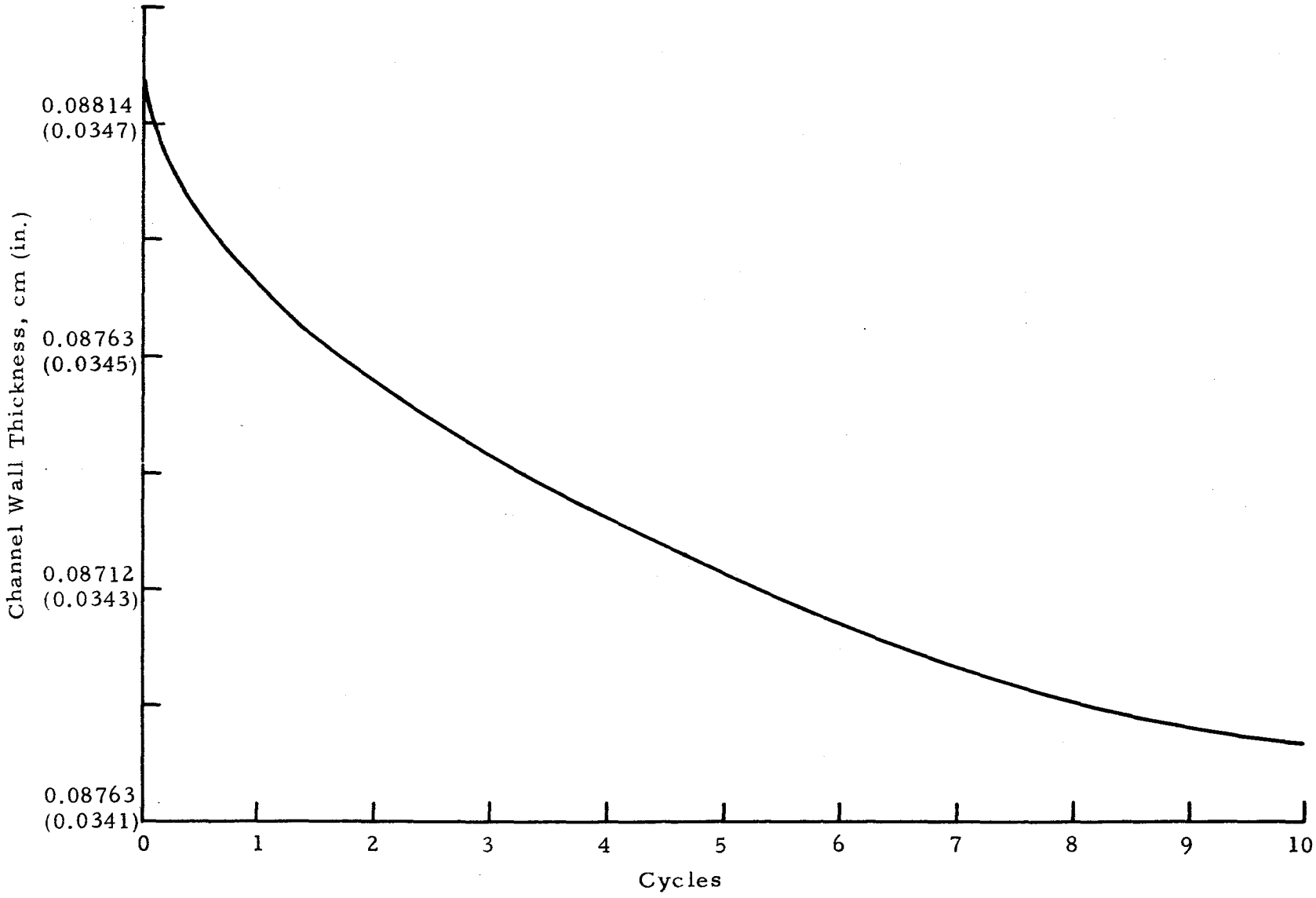

Fig. 34 - OFHC/EDNi Wall Thickness at Channel Centerline

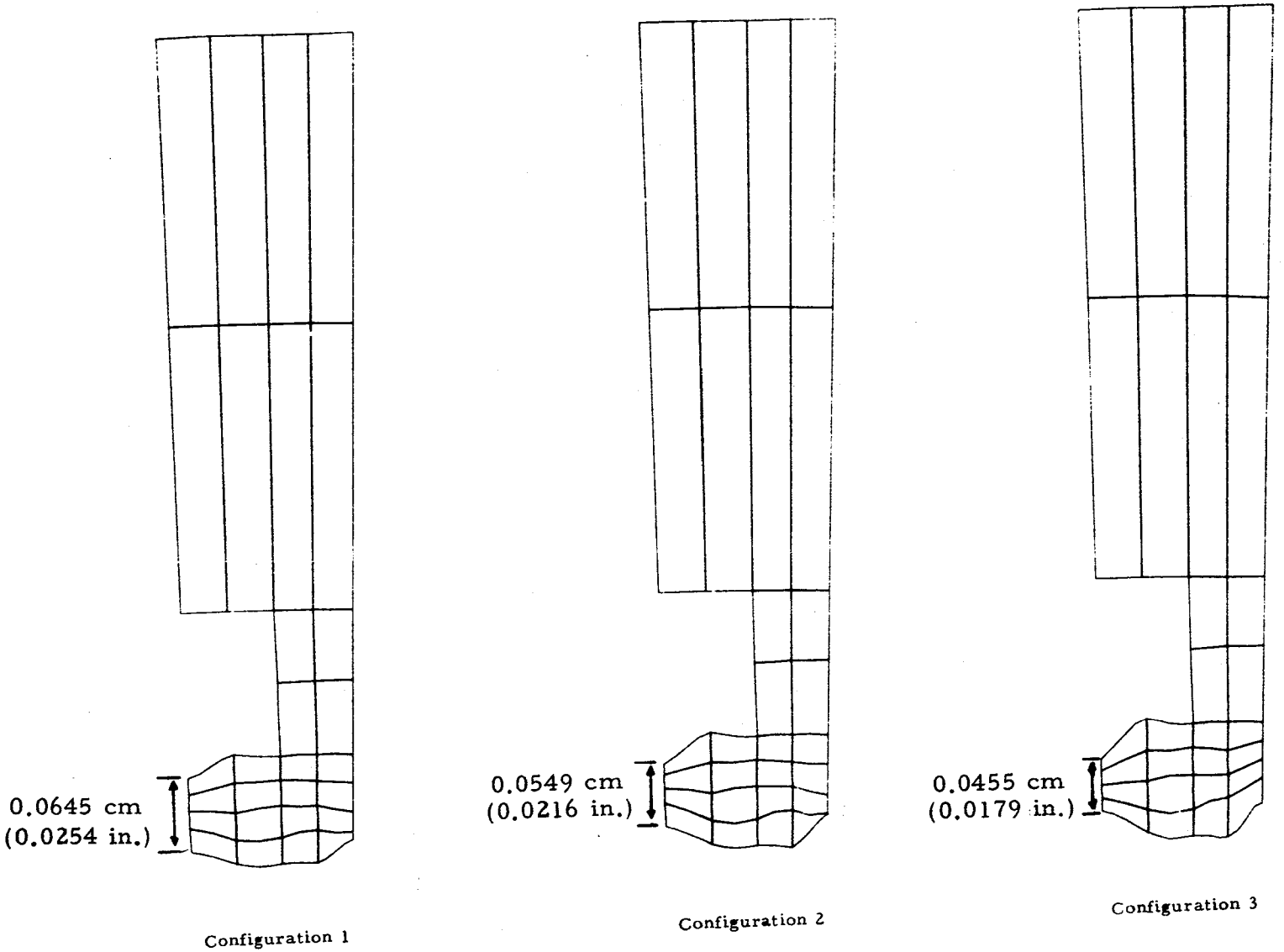

Fig. 35 - Computer Plots of Deformed OFHC/EFCU Models Used in Critical Geometry Analysis

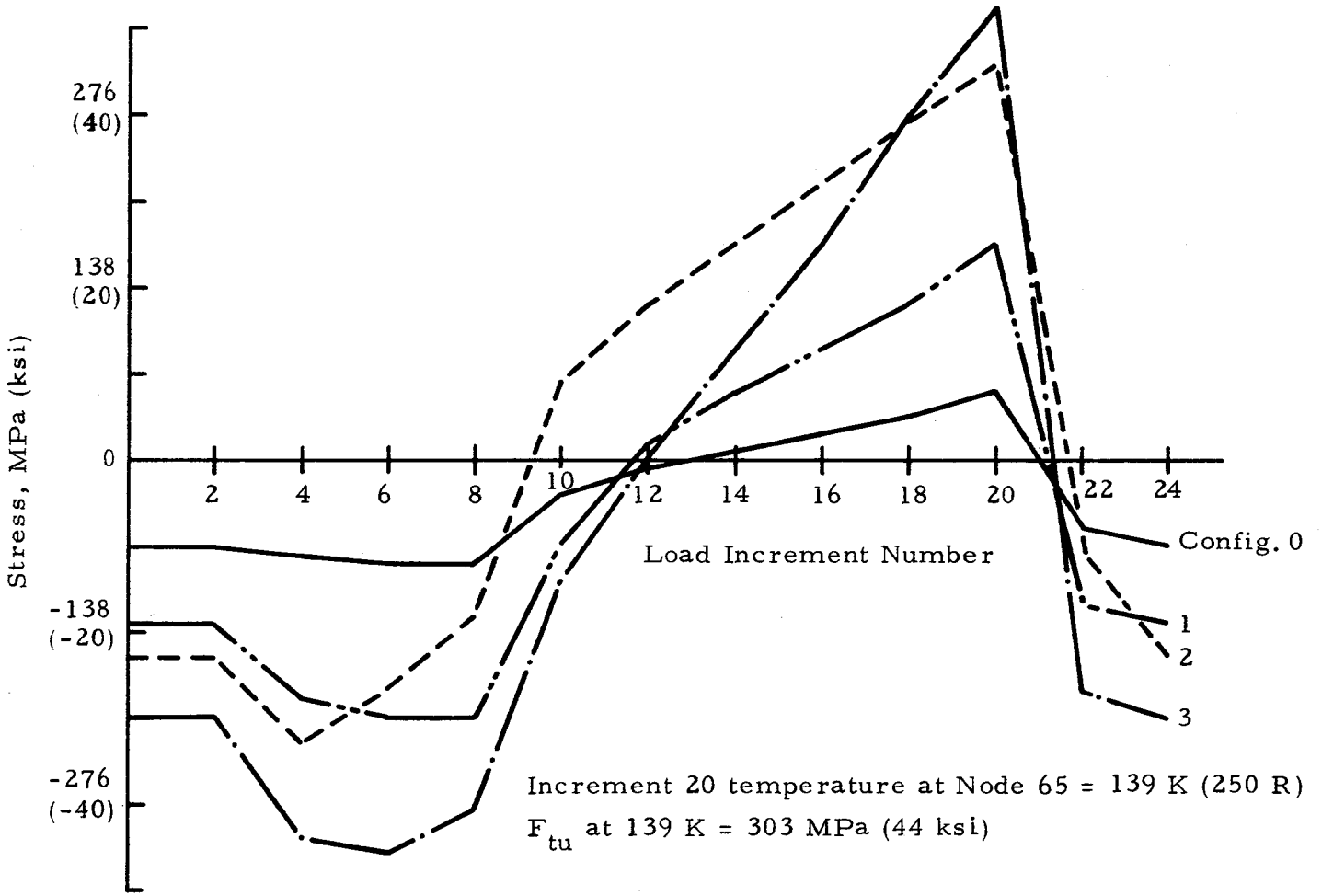

Fig. 36 - Computed Cyclic Hoop Stress at Node 65 in OFHC Chamber

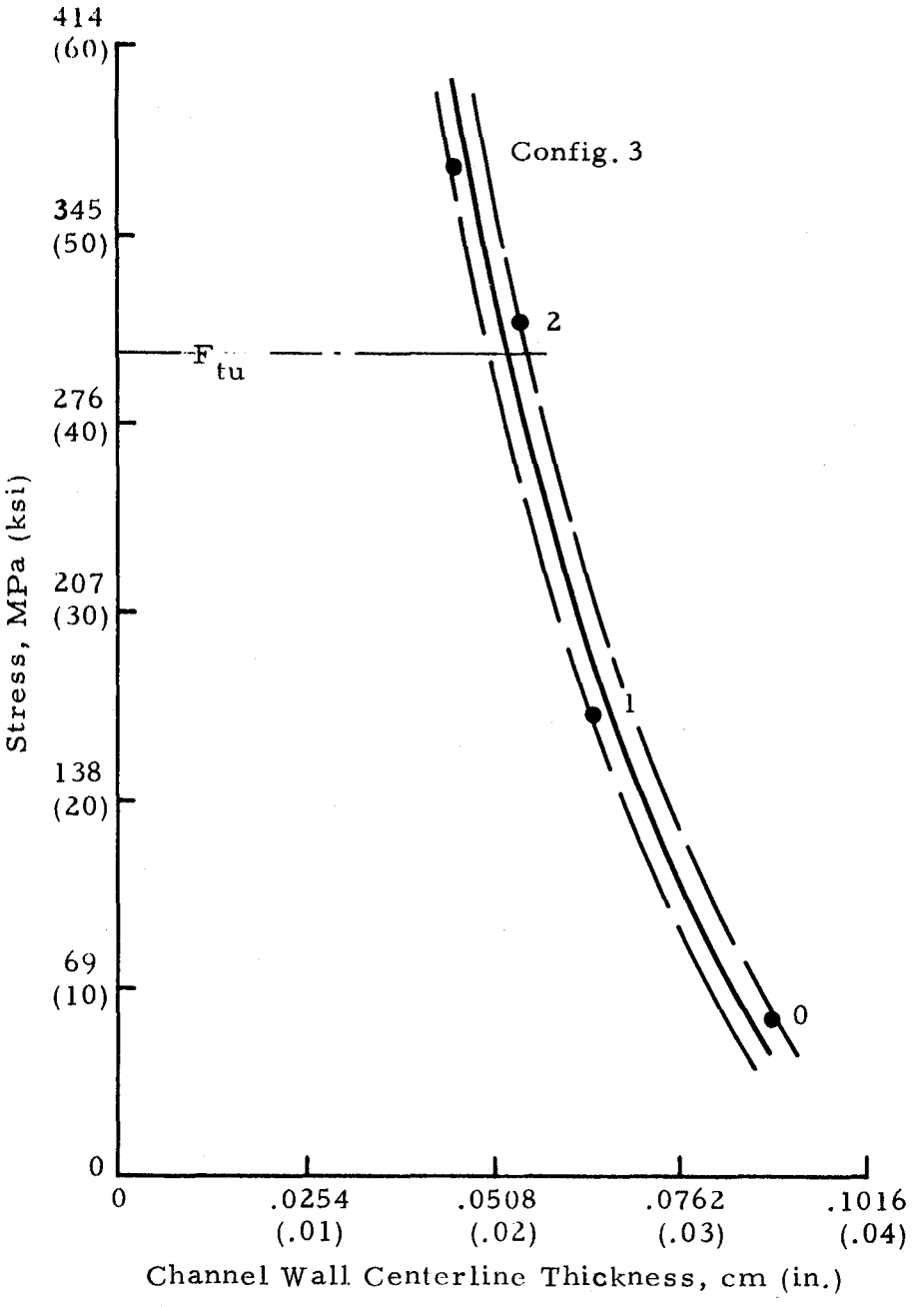

Fig. 37 - Maximum Hoop Stress at Channel Wall Centerline of Coolant Surface vs Channel Wall Thickness – OFHC Chamber

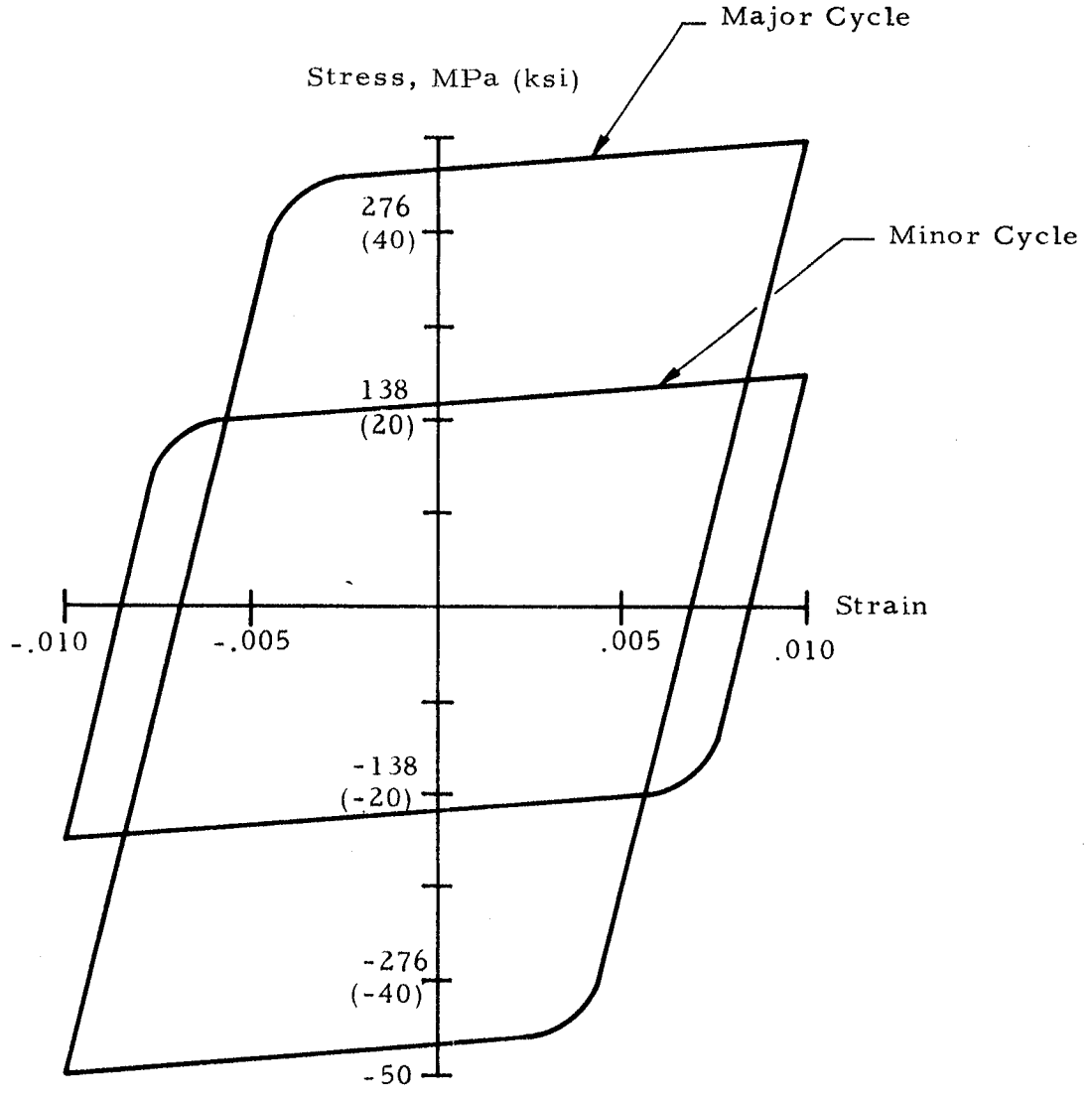

Fig. 38 - 28 K (50 R) Cyclic Stress Strain Curves for Isotropic Hardening Study

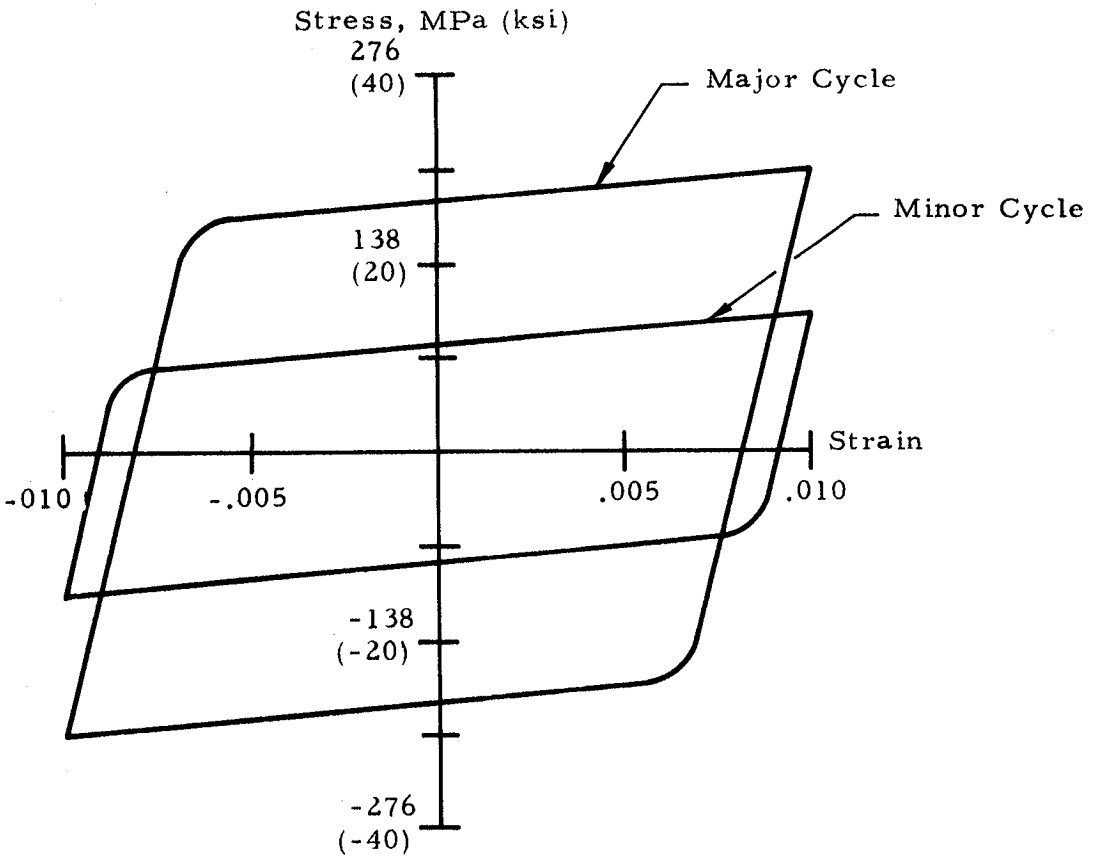

Fig. 39 - 861 K (1550 R) Cyclic Stress Strain Curves for Isotropic Hardening Study

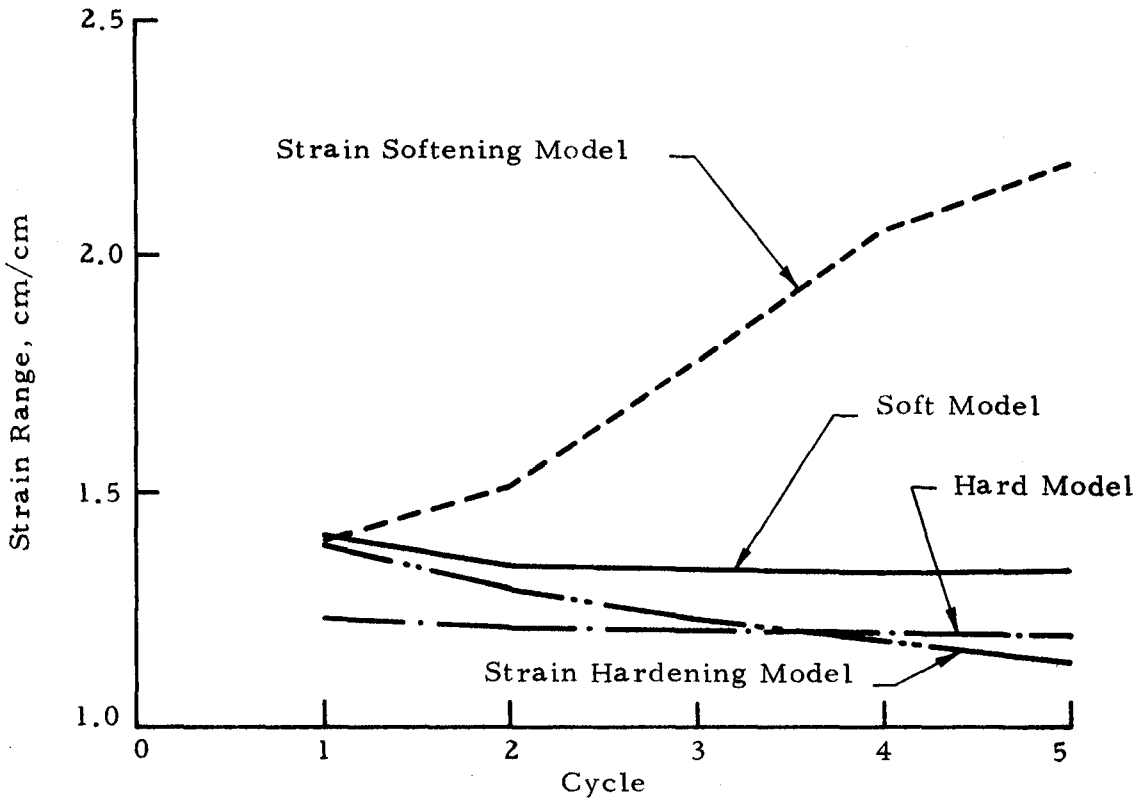

Fig. 40 - Effective Plastic Strain Range at Center of Element 16, Isotropic Hardening Effects

Node Id	Temperature, K (R)		
	Undeformed Config.	100-Cycle Config.	200-Cycle Config.
1	783 (1409)	776 (1397)	789 (1420)
9	797 (1435)	796 (1432)	813 (1463)
61	657 (1183)	659 (1186)	682 (1228)
65	699 (1258)	710 (1278)	729 (1313)
78	474 (853)	473 (852)	488 (879)
88	485 (873)	483 (870)	499 (898)

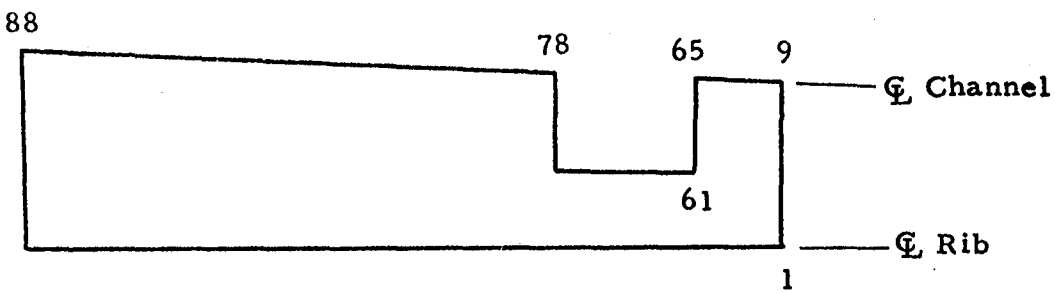

Node ID Locations

Fig. 41 - OFHC Structural Temperatures at the End of a Baseline Heating Phase (Time = 1.55 sec After Ignition)

NAS3-21953

DISTRIBUTION LIST FOR FINAL REPORT – CR 165241 (Vol. II) CR 165242 (Vol. III)

Name	No. of Copies
National Aeronautics and Space Administration Lewis Research Center 21000 BrookPark Rd. Cleveland, OH 44135	
Attn: Contracting Officer, MS 500-306	1
Technical Utilization Office, MS 7-3	1
Technical Report Control Office, MS 5-5	1
AFSC Liaison Office, MS 501-3	2
Library, MS 60-3	2
Office of Reliability & Quality Assurance, MS 500-211	1
N.T. Musial, MS 500-318	1
H.J. Kasper, Project Manager, MS 501-6	20
E.A. Bourke, MS 501-5	5
National Aeronautics and Space Administration Headquarters Washington, DC 20546	
Attn: Office of Aeronautics & Space Technology	
RS/Director, Manned Space Technology	1
RP/Director, Space Propulsion and Power	1
RW/Director, Materials & Structures	1
RP1/F.W. Stephenson	1
Attn: Office of Manned Space Flight	
MT/Director, Advanced Manned Mission	1
Attn: Office of Space Science	
SG/Director, Physics & Astronomy Programs	1
SL/Director, Planetary Programs	1
SV/Director, Launch Vehicles & Propulsion	1
Attn: Office of Technology Utilization Division	
KT/Director, Technology Utilization	1
National Aeronautics & Space Administration Ames Research Center Moffett Field, CA 94035	
Attn: Library	1
National Aeronautics & Space Administration Flight Research Center P.O. Box 273 Edwards, CA 93523	1

	No. of Copies
National Aeronautics and Space Administration George C. Marshall Space Flight Center Huntsville, AL 35912	
Attn: EP46/R. L. Hurford	1
EH23/W. B. McPherson	1
EP46/N. Schlemmer	1
EP21/J. A. Lombardo	1
EP23/R. H. Counts	1
National Aeronautics and Space Administration Goddard Space Flight Center Greenbelt, MD 20771	
Attn: Library	1
National Aeronautics and Space Administration John F. Kennedy Space Center Cocoa Beach, FL 32931	
Attn: Library	1
National Aeronautics and Space Administration Lyndon B. Johnson Space Center Houston,	
Attn: Library	1
National Aeronautics and Space Administration Langley Research Center Langley Station Hampton, VA 23365	
Attn: Library	1
NASA Scientific & Technical Information Facility P. O. Box 8757 Baltimore-Washington Intn'l. Airport Baltimore, MD 21240	
Attn: Accessioning Department	10
Office of the Director of Defense Research & Engineering Washington, DC 20301	
Attn: Office of Ass't Director (Chem. Technology)	1

No. of Copies

Jet Propulsion Laboratory
4800 Oak Grove Drive
Pasadena, CA 91103

Attn: Library 1
D. Dipprey 1
W. Ginn 1

Defense Documentation Center
Cameron Station, Bldg. 5
5010 Duke St.
Alexandria, VA 22314

Attn: TISIA 1

Advanced Research Projects Agency
Washington, DC 20525

Attn: Library 1

Aeronautical Systems Division
Air Force Systems Command
Wright-Patterson AFB, OH 45433

Attn: Library 1

Air Force Rocket Propulsion Laboratory (RPM)
Edwards, CA 93523

Attn: Library 1

Air Force FTC (FTAT-2)
Edwards Air Force Base, CA 93523

Attn: Library 1

Air Force Office of Scientific Research
1400 Wilson Blvd.
Arlington, VA 22209

Attn: Library 1

U.S. Air Force, Office of Information
Washington, DC 20333

Attn: Library 1

Air Force Aero Propulsion Laboratory
Research & Technology Division
U.S. Air Force Systems Command
Wright Patterson AFB, OH 45433

Attn: Library (APRP) 1

No. of Copies

Arnold Engineering Development Center
Air Force Systems Command
Tullahoma, TN

Attn: Library 1

Bureau of Naval Weapons
Department of the Navy
Washington, DC

Attn: Library 1

U.S. Naval Research Laboratory
Washington, DC 20390

Attn: Library 1

U.S. Army Research Office (Durham)
Box CM, Duke Station
Durham, NC 27706

Attn: Library 1

U.S. Army Missile Command
Redstone Scientific Information Center
Redstone Arsenal, AL 35808

Attn: Document Section 1

U.S. Naval Missile Center
Point Mugu, CA 93041

Attn: Technical Library 1

U.S. Naval Weapons Center
China Lake, CA 93557

Attn: Library 1

Aerojet Liquid Rocket Company
P.O. Box 13222
Sacramento, CA 95813

Attn: Technical Library 1
L. Bassham 1

Aro, Inc.
Arnold Engineering Development Center
Arnold AF Station, TN 37389

Attn: Library 1

	No. of Copies
Battelle Memorial Institute 505 King Avenue Columbus, OH 43201	
Attn: Library	1
Bell Aerosystems Inc. Box 1 Buffalo, NY 14240	
Attn: Library	1
Boeing Company, Space Division P.O. Box 868 Seattle, WA 98124	
Attn: Library	1
R.G. Voss	1
Chemical Propulsion Information Agency Applied Physics Laboratory 8621 Georgia Avenue Silver Spring, MD 20910	1
Chrysler Corporation Space Division P.O. Box 29200 New Orleans, LA 70129	
Attn: Library	1
General Electric Company Missiles & Space Systems Center Valley Forge Space Tech. Center P.O. Box 8555 Philadelphia, PA 19101	
Attn: Library	1
Grumman Aircraft Engineering Corp. Bethpage, L.I., NY 11714	
Attn: Library	1
Ling-Temco-Vought Corporation P.O. Box 5907 Dallas, TX 75222	
Attn: Library	1

	No. of Copies
Lockheed Missiles & Space Company P.O. Box 504 Sunnyvale, CA 93087	
Attn: Library	1
Marquardt Corporation 16555 Staticoy Street Box 2013 South Annex Van Nuys, CA 91409	
Attn: Library	1
Martin-Marietta Corp. P.O. Box 179 Denver, CO 80201	
Attn: Library	1
McDonnell Douglas Astronautics 5301 Bolsa Avenue Huntington Beach, CA 92647	
Attn: Library	1
Philco-Ford Corp. Aeronautics Div. Ford Rd. Newport Beach, CA 92663	
Attn: Library	1
Purdue University Lafayette, IN 47907	
Attn: Library	1
Rocketdyne A Div. of Rockwell Corp. 6633 Canoga Avenue Canoga Park, CA 91304	
Attn: Library N. Bergstresser	1 1
Rocket Research Corp. Willow Road at 116th Street Redmond, WA 98052	
Attn: Library	1

No. of Copies

Thiokol Chemical Corp.
P.O. Box 1000
Newton, PA 18940 — 1

TRW Systems, Inc.
1 Space Park
Redondo Beach, CA 90278

Attn: Library — 1

United Aircraft Corporation
Pratt & Whitney Division
Florida Research & Development Center
P.O. Box 2691
West Palm Beach, FL 33402

Attn: Library — 1

Amax Copper, Inc.
1270 Ave. of the Americas
New York, NY 10020

Attn: N. Kehl — 1
G.C. Van Tilburg — 1